Astronomy & Astrophysics manuscript no. aa39657e-20
February 18, 2022
©ESO 2022

arXiv:2012.01533v2 [astro-ph.GA] 9 Jun 2021

Gaia Early Data Release 3

Summary of the contents and survey properties

Gaia Collaboration, A.G.A. Brown[1], A. Vallenari[2], T. Prusti[3], J.H.J. de Bruijne[3], C. Babusiaux[4,5], M. Biermann[6], O.L. Creevey[7], D.W. Evans[8], L. Eyer[9], A. Hutton[10], F. Jansen[3], C. Jordi[11], S.A. Klioner[12], U. Lammers[13], L. Lindegren[14], X. Luri[11], F. Mignard[7], C. Panem[15], D. Pourbaix[16,17], S. Randich[18], P. Sartoretti[5], C. Soubiran[19], N.A. Walton[8], F. Arenou[5], C.A.L. Bailer-Jones[20], U. Bastian[6], M. Cropper[21], R. Drimmel[22], D. Katz[5], M.G. Lattanzi[22,23], F. van Leeuwen[8], J. Bakker[13], C. Cacciari[24], J. Castañeda[25], F. De Angeli[8], C. Ducourant[19], C. Fabricius[11], M. Fouesneau[20], Y. Frémat[26], R. Guerra[13], A. Guerrier[15], J. Guiraud[15], A. Jean-Antoine Piccolo[15], E. Masana[11], R. Messineo[27], N. Mowlavi[9], C. Nicolas[15], K. Nienartowicz[28,29], F. Pailler[15], P. Panuzzo[5], F. Riclet[15], W. Roux[15], G.M. Seabroke[21], R. Sordo[2], P. Tanga[7], F. Thévenin[7], G. Gracia-Abril[30,6], J. Portell[11], D. Teyssier[31], M. Altmann[6,32], R. Andrae[20], I. Bellas-Velidis[33], K. Benson[21], J. Berthier[34], R. Blomme[26], E. Brugaletta[35], P.W. Burgess[8], G. Busso[8], B. Carry[7], A. Cellino[22], N. Cheek[36], G. Clementini[24], Y. Damerdji[37,38], M. Davidson[39], L. Delchambre[37], A. Dell'Oro[18], J. Fernández-Hernández[40], L. Galluccio[7], P. García-Lario[13], M. Garcia-Reinaldos[13], J. González-Núñez[36,41], E. Gosset[37,17], R. Haigron[5], J.-L. Halbwachs[42], N.C. Hambly[39], D.L. Harrison[8,43], D. Hatzidimitriou[44], U. Heiter[45], J. Hernández[13], D. Hestroffer[34], S.T. Hodgkin[8], B. Holl[9,28], K. Janßen[46], G. Jevardat de Fombelle[9], S. Jordan[6], A. Krone-Martins[47,48], A.C. Lanzafame[35,49], W. Löffler[6], A. Lorca[10], M. Manteiga[50], O. Marchal[42], P.M. Marrese[51,52], A. Moitinho[47], A. Mora[10], K. Muinonen[53,54], P. Osborne[8], E. Pancino[18,52], T. Pauwels[26], J.-M. Petit[55], A. Recio-Blanco[7], P.J. Richards[56], M. Riello[8], L. Rimoldini[28], A.C. Robin[55], T. Roegiers[57], J. Rybizki[20], L.M. Sarro[58], C. Siopis[16], M. Smith[21], A. Sozzetti[22], A. Ulla[59], E. Utrilla[10], M. van Leeuwen[8], W. van Reeven[10], U. Abbas[22], A. Abreu Aramburu[40], S. Accart[60], C. Aerts[61,62,20], J.J. Aguado[58], M. Ajaj[5], G. Altavilla[51,52], M.A. Álvarez[63], J. Álvarez Cid-Fuentes[64], J. Alves[65], R.I. Anderson[66], E. Anglada Varela[40], T. Antoja[11], M. Audard[28], D. Baines[31], S.G. Baker[21], L. Balaguer-Núñez[11], E. Balbinot[67], Z. Balog[6,20], C. Barache[32], D. Barbato[9,22], M. Barros[47], M.A. Barstow[68], S. Bartolomé[11], J.-L. Bassilana[60], N. Bauchet[34], A. Baudesson-Stella[60], U. Becciani[35], M. Bellazzini[24], M. Bernet[11], S. Bertone[69,70,22], L. Bianchi[71], S. Blanco-Cuaresma[72], T. Boch[42], A. Bombrun[73], D. Bossini[74], S. Bouquillon[32], A. Bragaglia[24], L. Bramante[27], E. Breedt[8], A. Bressan[75], N. Brouillet[19], B. Bucciarelli[22], A. Burlacu[76], D. Busonero[22], A.G. Butkevich[22], R. Buzzi[22], E. Caffau[5], R. Cancelliere[77], H. Cánovas[10], T. Cantat-Gaudin[11], R. Carballo[78], T. Carlucci[32], M.I Carnerero[22], J.M. Carrasco[11], L. Casamiquela[19], M. Castellani[51], A. Castro-Ginard[11], P. Castro Sampol[11], L. Chaoul[15], P. Charlot[19], L. Chemin[79], A. Chiavassa[7], M.-R. L. Cioni[46], G. Comoretto[80], W.J. Cooper[81,22], T. Cornez[60], S. Cowell[8], F. Crifo[5], M. Crosta[22], C. Crowley[73], C. Dafonte[63], A. Dapergolas[33], M. David[82], P. David[34], P. de Laverny[7], F. De Luise[83], R. De March[27], J. De Ridder[61], R. de Souza[84], P. de Teodoro[13], A. de Torres[73], E.F. del Peloso[6], E. del Pozo[10], M. Delbo[7], A. Delgado[8], H.E. Delgado[58], J.-B. Delisle[9], P. Di Matteo[5], S. Diakite[85], C. Diener[8], E. Distefano[35], C. Dolding[21], D. Eappachen[86,62], B. Edvardsson[87], H. Enke[46], P. Esquej[88], C. Fabre[89], M. Fabrizio[51,52], S. Faigler[90], G. Fedorets[53,91], P. Fernique[42,92], A. Fienga[93,34], F. Figueras[11], C. Fouron[76], F. Fragkoudi[94], E. Fraile[88], F. Franke[95], M. Gai[22], D. Garabato[63], A. Garcia-Gutierrez[11], M. García-Torres[96], A. Garofalo[24], P. Gavras[88], E. Gerlach[12], R. Geyer[12], P. Giacobbe[22], G. Gilmore[8], S. Girona[64], G. Giuffrida[51], R. Gomel[90], A. Gomez[63], I. Gonzalez-Santamaria[63], J.J. González-Vidal[11], M. Granvik[53,97], R. Gutiérrez-Sánchez[31], L.P. Guy[28,80], M. Hauser[20,98], M. Haywood[5], A. Helmi[67], S.L. Hidalgo[99,100], T. Hilger[12], N. Hładczuk[13], D. Hobbs[14], G. Holland[8], H.E. Huckle[21], G. Jasniewicz[101], P.G. Jonker[62,86], J. Juaristi Campillo[6], F. Julbe[11], L. Karbevska[9], P. Kervella[102], S. Khanna[67], A. Kochoska[103], M. Kontizas[44], G. Kordopatis[7], A.J. Korn[45], Z. Kostrzewa-Rutkowska[1,86], K. Kruszyńska[104], S. Lambert[32], A.F. Lanza[35], Y. Lasne[60], J.-F. Le Campion[105], Y. Le Fustec[76], Y. Lebreton[102,106], T. Lebzelter[65], S. Leccia[107], N. Leclerc[5], I. Lecoeur-Taibi[28], S. Liao[22], E. Licata[22], H.E.P. Lindstrøm[22,108], T.A. Lister[109], E. Livanou[44], A. Lobel[26], P. Madrero Pardo[11], S. Managau[60], R.G. Mann[39], J.M. Marchant[110], M. Marconi[107], M.M.S. Marcos Santos[36], S. Marinoni[51,52], F. Marocco[111,112], D.J. Marshall[113], L. Martin Polo[36], J.M. Martín-Fleitas[10], A. Masip[11], D. Massari[24], A. Mastrobuono-Battisti[14], T. Mazeh[90], P.J. McMillan[14], S.

Messina[35], D. Michalik[3], N.R. Millar[8], A. Mints[46], D. Molina[11], R. Molinaro[107], L. Molnár[114,115,116], P. Montegriffo[24], R. Mor[11], R. Morbidelli[22], T. Morel[37], D. Morris[39], A.F. Mulone[27], D. Munoz[60], T. Muraveva[24], C.P. Murphy[13], I. Musella[107], L. Noval[60], C. Ordénovic[7], G. Orrù[27], J. Osinde[88], C. Pagani[68], I. Pagano[35], L. Palaversa[117,8], P.A. Palicio[7], A. Panahi[90], M. Pawlak[118,104], X. Peñalosa Esteller[11], A. Penttilä[53], A.M. Piersimoni[83], F.-X. Pineau[42], E. Plachy[114,115,116], G. Plum[5], E. Poggio[22], E. Poretti[119], E. Poujoulet[120], A. Prša[103], L. Pulone[51], E. Racero[36,121], S. Ragaini[24], M. Rainer[18], C.M. Raiteri[22], N. Rambaux[34], P. Ramos[11], M. Ramos-Lerate[122], P. Re Fiorentin[22], S. Regibo[61], C. Reylé[55], V. Ripepi[107], A. Riva[22], G. Rixon[8], N. Robichon[5], C. Robin[60], M. Roelens[9], L. Rohrbasser[28], M. Romero-Gómez[11], N. Rowell[39], F. Royer[5], K.A. Rybicki[104], G. Sadowski[16], A. Sagristà Sellés[6], J. Sahlmann[88], J. Salgado[31], E. Salguero[40], N. Samaras[26], V. Sanchez Gimenez[11], N. Sanna[18], R. Santoveña[63], M. Sarasso[22], M. Schultheis[7], E. Sciacca[35], M. Segol[95], J.C. Segovia[36], D. Ségransan[9], D. Semeux[89], S. Shahaf[90], H.I. Siddiqui[123], A. Siebert[42,92], L. Siltala[53], E. Slezak[7], R.L. Smart[22], E. Solano[124], F. Solitro[27], D. Souami[102,125], J. Souchay[32], A. Spagna[22], F. Spoto[72], I.A. Steele[110], H. Steidelmüller[12], C.A. Stephenson[31], M. Süveges[28,126,20], L. Szabados[114], E. Szegedi-Elek[114], F. Taris[32], G. Tauran[60], M.B. Taylor[127], R. Teixeira[84], W. Thuillot[34], N. Tonello[64], F. Torra[25], J. Torra†[11], C. Turon[5], N. Unger[9], M. Vaillant[60], E. van Dillen[95], O. Vanel[5], A. Vecchiato[22], Y. Viala[5], D. Vicente[64], S. Voutsinas[39], M. Weiler[11], T. Wevers[8], Ł. Wyrzykowski[104], A. Yoldas[8], P. Yvard[95], H. Zhao[7], J. Zorec[128], S. Zucker[129], C. Zurbach[130], and T. Zwitter[131]

(Affiliations can be found after the references)

Received ; accepted

ABSTRACT

Context. We present the early installment of the third *Gaia* data release, *Gaia* EDR3, consisting of astrometry and photometry for 1.8 billion sources brighter than magnitude 21, complemented with the list of radial velocities from *Gaia* DR2.

Aims. A summary of the contents of *Gaia* EDR3 is presented, accompanied by a discussion on the differences with respect to *Gaia* DR2 and an overview of the main limitations which are present in the survey. Recommendations are made on the responsible use of *Gaia* EDR3 results.

Methods. The raw data collected with the *Gaia* instruments during the first 34 months of the mission have been processed by the *Gaia* Data Processing and Analysis Consortium (DPAC) and turned into this early third data release, which represents a major advance with respect to *Gaia* DR2 in terms of astrometric and photometric precision, accuracy, and homogeneity.

Results. *Gaia* EDR3 contains celestial positions and the apparent brightness in G for approximately 1.8 billion sources. For 1.5 billion of those sources, parallaxes, proper motions, and the $(G_{\rm BP} - G_{\rm RP})$ colour are also available. The passbands for G, $G_{\rm BP}$, and $G_{\rm RP}$ are provided as part of the release. For ease of use, the 7 million radial velocities from *Gaia* DR2 are included in this release, after the removal of a small number of spurious values. New radial velocities will appear as part of *Gaia* DR3. Finally, *Gaia* EDR3 represents an updated materialisation of the celestial reference frame (CRF) in the optical, the *Gaia*-CRF3, which is based solely on extragalactic sources. The creation of the source list for *Gaia* EDR3 includes enhancements that make it more robust with respect to high proper motion stars, and the disturbing effects of spurious and partially resolved sources. The source list is largely the same as that for *Gaia* DR2, but it does feature new sources and there are some notable changes. The source list will not change for *Gaia* DR3.

Conclusions. *Gaia* EDR3 represents a significant advance over *Gaia* DR2, with parallax precisions increased by 30 per cent, proper motion precisions increased by a factor of 2, and the systematic errors in the astrometry suppressed by 30–40% for the parallaxes and by a factor ~ 2.5 for the proper motions. The photometry also features increased precision, but above all much better homogeneity across colour, magnitude, and celestial position. A single passband for G, $G_{\rm BP}$, and $G_{\rm RP}$ is valid over the entire magnitude and colour range, with no systematics above the 1% level.

Key words. catalogs - astrometry - parallaxes - proper motions - techniques: photometric - techniques: radial velocities

1. Introduction

We present the first installment of the third intermediate *Gaia* data release, *Gaia* Early Data Release 3 (*Gaia* EDR3), which is based on the data collected during the first 34 months of the mission. This early part of *Gaia* DR3 consists of an updated source list, astrometry, and broad band photometry in the G, $G_{\rm BP}$, and $G_{\rm RP}$ bands. In addition, an updated list of radial velocities from *Gaia* DR2, cleaned from spurious values, is included. *Gaia* EDR3 represents a significant improvement in both the precision and accuracy of the astrometry and broad-band photometry. The factor two improvement in proper motion precision provides new views of the fine structure of Galactic phase space. The suppression of systematic errors enables, for the first time, a measurement in the optical of the acceleration of the solar system barycentre with respect to the rest frame of distant extragalactic sources (Gaia Collaboration et al. 2021c), which is a beautiful confirmation of the superb astrometric quality of *Gaia* EDR3. Likewise, the photometry is significantly improved over *Gaia* DR2; it is much more homogeneous over the sky, as well as over source brightness and colour, where a single passband for G, $G_{\rm BP}$, and $G_{\rm RP}$ can now be used over the entire magnitude and colour range, with no systematics above the 1% level.

The full *Gaia* DR3 release is expected in 2022 and will enrich the current release with the following: updated and new radial velocities; astrophysical parameters for sources based on the blue and red prism photometer (BP and RP) spectra, as well as spectra from the radial velocity spectrograph (RVS); the mean BP and RP prism- and RVS-spectra for a subset of sources; an

extended catalogue of variable stars; the first catalogue of binary stars, including eclipsing, spectroscopic, and astrometric binaries; astrometry for a larger sample of solar system objects, and reflectance spectra for a small subset of asteroids; quasi-stellar object (QSO) host and galaxy morphological characterisation; and the light curves for all sources in a field centred on M31. We stress here that the source list, astrometry, and broad-band photometry will not be updated from *Gaia* EDR3 to *Gaia* DR3, both releases being based on the same number of input observations.

This paper is structured as follows. In Sect. 2 we provide a short overview of the improvements and additions to the data processing that led to the production of *Gaia* EDR3. We summarise the contents of the early installment of the third data release in Sect. 3 and comment on the quality of this release in Sect. 4. In Sect. 5 we discuss the major differences between *Gaia* EDR3 and *Gaia* DR2. In Sect. 6 we comment on the completeness of *Gaia* EDR3 and some of the known limitations which the user of the data should keep in mind. Additional guidance on the use of *Gaia* EDR3 is provided in Sect. 7. In Sect. 8 we provide updates to the *Gaia* data access facilities and documentation available to the astronomical community. *Gaia* started collecting scientific data in July 2014 (Gaia Collaboration et al. 2016b) and is currently in its extended mission phase, the nominal 60 month mission having been concluded on July 16, 2019. We conclude with a look ahead at the extended *Gaia* mission and the next data releases in Sect. 9. Throughout the paper we make reference to other *Gaia* Collaboration and *Gaia* Data Processing and Analysis Consortium (DPAC) papers that provide more details on the data processing and validation for *Gaia* EDR3. All these papers (together with the present article) can be found in the Astronomy & Astrophysics Special issue on *Gaia* EDR3.

2. Data processing for *Gaia* EDR3

As described in detail in Gaia Collaboration et al. (2016b), *Gaia* measurements are collected with three instruments. The astrometric instrument collects images in *Gaia*'s white-light G-band (330–1050 nm); the blue (BP) and red (RP) prism photometers collect low resolution spectrophotometric measurements of source spectral energy distributions over the wavelength ranges 330–680 nm and 640–1050 nm, respectively; and the radial velocity spectrometer (RVS) collects medium resolution ($R \sim 11\,700$) spectra over the wavelength range 845–872 nm centred on the Calcium triplet region (Cropper et al. 2018).

We repeat here for convenience the way events on board *Gaia*, including the data collection, are timed. The times are given in terms of the on board mission timeline (OBMT) which is generated by the *Gaia* on board clock. By convention OBMT is expressed in units of six hour (21 600 s) spacecraft revolutions (Gaia Collaboration et al. 2016b). The approximate relation between OBMT (in revolutions) and barycentric coordinate time (TCB, in Julian years) at *Gaia* is

$$\mathrm{TCB} \simeq \mathrm{J2015.0} + (\mathrm{OBMT} - 1717.6256\,\mathrm{rev})/(1461\,\mathrm{rev\,yr^{-1}})\,. \quad (1)$$

The 34 month time interval covered by the observations used for *Gaia* EDR3 starts at OBMT 1078.3795 rev = J2014.5624599 TCB (approximately July 25, 2014, 10:30:00 UTC), and ends at OBMT 5230.0880 rev = J2017.4041495 TCB (approximately May 28, 2017, 08:45:00 UTC). This time interval contains gaps caused by both spacecraft events and by on-ground data processing problems. This leads to gaps in the data collection or stretches of time over which the input data cannot be used. Which data are considered unusable varies across the *Gaia* data processing systems (here astrometry and photometry), and as a consequence the effective amount of input data used differs from one system to the other. We refer to the specific *Gaia* EDR3 data processing papers (listed below) for the details.

The pre-processing for all *Gaia* instruments is described in Hambly et al. (2018) and includes the removal of the effects of non-uniformity of the charge-coupled device (CCD) bias levels. A summary of the entire data processing system for *Gaia* is given in Gaia Collaboration et al. (2016b). The sub-sections below summarise the major improvements in the data processing for *Gaia* EDR3 with respect to *Gaia* DR2.

2.1. Source list

A given data processing cycle for *Gaia* starts with the creation of the list of sources that will be treated. The series of CCD measurements recorded as a source travels across the focal plane (referred to collectively as a "transit", Torra et al. 2021), are grouped and assigned to known sources on the sky or to newly "created" sources, corresponding to groups of transits at a celestial position where previously no source was catalogued. The starting point for creating the source list is the previous *Gaia* data release, or the Initial *Gaia* Source List (Smart & Nicastro 2014) in the case of *Gaia* DR1. As pointed out in Gaia Collaboration et al. (2018) the source list may evolve from one release to the next due to the merging of groups of transits previously assigned to two or more sources, the splitting of a group of transits into two or more sources, or changing the list of transits assigned to a source. The changes in the source list from *Gaia* DR1 to *Gaia* DR2 were significant but from *Gaia* DR2 to *Gaia* EDR3 the source list has largely stabilised, the changes being at the 2–3 per cent level overall.

A full account of how the source list is created for *Gaia* EDR3 (and *Gaia* DR3) can be found in Torra et al. (2021), who note the following significant improvements with respect to *Gaia* DR2. The identification of spurious on-board detections (caused among others by bright star diffraction spikes, bright cosmic rays, or major planets in the solar system transiting across or near a telescope field of view) has been improved which leads to a much cleaner list of sources and associated transits.

The algorithm that groups together transits and assigns them to sources has been improved with respect to the treatment of high-proper motion stars and variable stars. High proper motion stars are seen as groups of observations stretched out over the sky which were mistaken for multiple sources in previous releases. They are now reliably recognised as belonging to the same source. The grouping of transits and their association to sources contains a stage where the magnitude of the source observed during a transit is taken into account. For highly variable sources this can lead to a splitting of the transits over multiple sources. This type of error is now prevented through a post-processing step which can recognise clusters of detections very close together on the sky, but disjoint in time, as belonging to the same (variable) source.

A more comprehensive analysis and cleaning of the observation-to-source matching results led to less sources with highly significant negative parallaxes or too large parallaxes (see appendix C in Lindegren et al. 2018), which also removes spuriously high proper motions. The treatment of close source pairs was improved to deal with the pairs with separations below 400 mas which were erroneously considered duplicate sources in *Gaia* DR2. These now appear as two sources in *Gaia* EDR3.

The separation limit below which two sources are considered duplicates was lowered to 180 mas.

For quantitative information on the above please refer to Torra et al. (2021). We stress here that the source list for *Gaia* EDR3 and *Gaia* DR3 will be the same and thus the process described in Torra et al. (2021) applies to both releases.

2.2. Astrometric data processing improvements

The astrometric processing for *Gaia* EDR3 is described in Lindegren et al. (2021b), who note the following major improvements with respect to the processing for *Gaia* DR2. The basic inputs for the Astrometric Global Iterative Solution (AGIS; Lindegren et al. 2012) are the source image locations in the *Gaia* CCD pixel stream, translated to observation times and across-scan locations. The image locations are determined in a process called "image parameter determination" (IPD; Rowell et al. 2021), by fitting a point spread function (PSF) or line spread function (LSF) to the 2D or 1D observation windows containing the image samples. The modelling of the PSF and LSF has been very much improved with the introduction of time and source colour dependencies, among many other enhancements. The details are described in Rowell et al. (2021). It is shown in Lindegren et al. (2021b) that for sources fainter than $G = 13$ the chromatic effects on image locations are almost completely removed during the image parameter determination stage, thus mostly eliminating an important source of systematic errors. Eventually for future *Gaia* data releases this should remove the need for colour terms in the astrometric calibrations. The colour of a source is included in the form of the effective wave number $\nu_{\rm eff}$, which is derived from the flux as a function of wavelength in the BP and RP prism spectra.

For the first time the image parameter determination and astrometric solution were iterated. Specifically, after the first IPD run an AGIS solution was produced, which was then used to improve the PSF and LSF calibrations for a second round of IPD (which benefits from improved source positions from the first AGIS run), followed by the *Gaia* EDR3 production run of AGIS. This leads to a more self-consistent set of image locations and source astrometric parameters. In addition, the image fluxes estimated as part of the IPD are improved, which in turn improves the *G*-band photometric processing. A diagram illustrating this data processing flow can be found in Lindegren et al. (2021b).

The astrometric calibration model was improved and extended. Several new dependencies were introduced to better handle the locations of saturated images, the effects of charge transfer inefficiency, and imperfections in the PSF and LSF models that leave residual effects at the sub-pixel level, and as a function of the rate at which sources move across the telescope field of view, perpendicular to the scan direction (caused by the spin axis precession of *Gaia*).

The *Gaia* EDR3 astrometric processing includes a model (Velocity error and effective Basic Angle Calibration, VBAC) that can calibrate out the effects of spin-related instrument distortions, in particular distortions over time scales comparable to the six hour spin period of *Gaia*. An important component of these distortions are the basic angle variations, of which the term proportional to the cosine of the spacecraft spin phase Ω can lead to a global parallax bias if left uncorrected (Butkevich et al. 2017). The VBAC model introduces additive corrections to the basic angle variation corrections calculated on the basis of the basic angle monitor measurements (cf. Lindegren et al. 2018). Lindegren et al. (2021b) describe the successful attempt to fit the coefficient of the $\cos\Omega$ term, which leads to a reduction in the size of the overall parallax zero point, which for *Gaia* EDR3 is -17 μas (compared to -29 μas for *Gaia* DR2), as estimated from quasar parallaxes.

An additional calibration model, which handles telescope focal length and optical distortion variations over smaller scales than handled by VBAC, was introduced to further reduce instrument distortion related systematics. Lastly, an ad-hoc correction was introduced to ensure that the bright star reference frame has no net spin with respect to the reference frame defined by quasars, an issue that was described in detail in Lindegren et al. (2018) and Lindegren (2020a,b).

Overall the *Gaia* EDR3 astrometry shows a reduction in the median uncertainties at $G = 15$ by a factor 0.71 for the positions and parallaxes and 0.44 for the proper motions. At the bright end ($G < 12$) the gain is larger, a factor 0.43 for positions and parallaxes and 0.27 for the proper motions, thanks to much improved calibrations. The overall parallax zero point has improved as mentioned above, and the variance over the sky in the systematic errors (as estimated from quasars) has been reduced by 30–40% for the parallaxes and by a factor of ~ 2.5 for proper motions. Lindegren et al. (2021b,a) provide many more details (see also Sect. 7.1).

2.3. Photometric data processing improvements

The photometric data processing for *Gaia* EDR3 is described in Riello et al. (2021), where only the processing for the broad band photometry is considered. The processing and calibration of the spectra will be described in forthcoming papers (De Angeli et al. 2021; Carrasco et al. 2021; Montegriffo et al. 2021). The BP and RP spectra are still being validated internally to DPAC at the time of the *Gaia* EDR3 release, by employing them in the astrophysical characterisation of sources. The spectra will be published as part of *Gaia* DR3 (for a subset of sources only). Riello et al. (2021) describe the following improvements to the broad-band photometric processing.

The *G*-band photometry benefits from the improvements implemented for the astrometric instrument image parameter determination stage. As described in Rowell et al. (2021), this includes a better PSF and LSF modelling, better treatment of saturated images, the masking out of suspected disturbing sources and a more precise determination of the background flux for each observation window. This leads to more accurate and robust *G*-band flux estimates.

The broad band photometry benefits from a detailed evaluation of the observations potentially affected by neighbouring sources in crowded fields. Although the crowding effects were not corrected, the crowding evaluation led to a cleaner list of internal calibration sources. The background flux in BP and RP due to stray light and astronomical sources is better determined, with higher spatial resolution to follow smaller scale variations.

The range of time over which observations free from telescope throughput losses (due to contamination; Gaia Collaboration et al. 2016b) are available was much extended. This allowed for better sky coverage of internal calibrator sources and more flexibility to select an optimal set of calibrators, well distributed in colour and magnitude. The external calibration used to determine the passbands is based on a much larger set of calibrators, covering a wider spectral range, where in *Gaia* DR2 only the spectrophotometric standard stars (Pancino et al. 2012) were used which limited the aspects of the passbands that could be determined reliably.

These improvements, and the larger set of input observations, have led to broad-band photometry which is significantly

Table 1. Number of sources of a certain type, or the number of sources for which a given data product is available in *Gaia* EDR3.

Data product or source type	Number of sources
Total	1 811 709 771
5-parameter astrometry	585 416 709
6-parameter astrometry	882 328 109
2-parameter astrometry	343 964 953
Gaia-CRF3 sources	1 614 173
ICRF3 sources for frame orientation	2269
Gaia-CRF3 sources for frame spin	429 249
G-band	1 806 254 432
G_{BP}-band	1 542 033 472
G_{RP}-band	1 554 997 939
Radial velocity	7 209 831

Table 2. Distribution of the *Gaia* EDR3 sources in *G*-band magnitude.

Magnitude distribution percentiles (G)					
Percentile	All	5-p	6-p	2-p	v_{rad}
0.135%	11.7	10.6	15.1	15.7	6.7
2.275%	15.1	13.7	17.4	18.8	9.2
15.866%	17.9	16.3	18.9	20.1	11.2
50%	19.7	18.1	19.9	20.7	12.4
84.134%	20.6	19.4	20.5	21.0	13.2
97.725%	21.0	20.4	20.8	21.2	14.1
99.865%	21.5	20.8	20.9	21.7	15.1

Notes. The distribution percentiles are shown for all sources and for those with a 5-p, 6-p, and 2-p astrometric solution, respectively, as well as the sources for which a radial velocity is available in *Gaia* EDR3.

better than *Gaia* DR2 photometry in both precision and accuracy. Especially at the bright end ($G < 13$) large gains were made, and many of the systematic effects reported for *Gaia* DR2, such as imprints from the zodiacal light and the scan law features (Evans et al. 2018; Arenou et al. 2018), have been removed or greatly suppressed (cf. Fabricius et al. 2021). In addition the problem that two passbands are needed to describe the *Gaia* DR2 *G*-band photometry (Maíz Apellániz & Weiler 2018) has been resolved, with only one passband needed for *Gaia* EDR3 for each of *G*, G_{BP}, and G_{RP}.

Despite the improvements in the astrometry and photometry, several limitations remain in *Gaia* EDR3 which require taking care when using the data. In Sect. 6 we summarise the known limitations of the present *Gaia* data release and point out, where relevant, the causes. In Sect. 7, and in Lindegren et al. (2021b) (astrometry), Riello et al. (2021) (photometry), and Fabricius et al. (2021) (catalogue validation) we provide additional guidance on the use of *Gaia* EDR3 results. The reader is strongly encouraged to read these papers and the online documentation[1] to understand the limitations in detail.

3. Overview of the contents of *Gaia* EDR3

Gaia EDR3 contains new astrometry and broad-band photometry, as well as radial velocities from *Gaia* DR2. Basic statistics on the source numbers and the overall distribution in *G* can be found in Tables 1 and 2. The overall quality of *Gaia* EDR3 results in terms of the typically achieved uncertainties is summarised in Table 3. The contents of the main components of the release, of which the magnitude distributions are shown in Figs. 1 and 2, are summarised in the following.

3.1. Astrometric data set

The astrometric data in *Gaia* EDR3 comprises three subsets:

5-parameter solutions (5-p). For these sources the colour information (ν_{eff} derived during the processing for *Gaia* DR2) was of high enough quality to assume that any chromatic effects were removed during the IPD stage, thus allowing for a standard 5-parameter (α, δ, ϖ, $\mu_{\alpha*}$, μ_δ) astrometric solution.

6-parameter solutions (6-p). For these sources no colour information of sufficient quality was available, thus forcing an estimate of the image locations with a PSF or LSF model for a default source colour. This means that chromatic effects have to be accounted for in the astrometric solution by estimating ν_{eff} for the source along with the astrometric parameters. Thus for these sources the 5 astrometric parameters and the so-called pseudo-colour are published along with a 6×6 covariance matrix listing, in addition to the astrometric covariance matrix entries, the uncertainty on the pseudo-colour and the correlations between the estimated colour and the astrometric parameters.

2-parameter solutions (2-p). As for previous releases there are sources for which insufficient data of the required quality is available to justify publishing a full 5-p or 6-p solution. For these sources a 5- or 6-parameter solution is in fact made, but with so-called galactic priors on the parallaxes and proper motions (Michalik et al. 2015; Lindegren et al. 2018, the fall-back solution). Only the positions and their covariance matrix are published for these sources. In principle all sources at $G > 21$ have a 2-p solution. However this boundary is not strict because the limit in *G* was decided on the basis of the *Gaia* DR2 value for the magnitude or that based on the on-board estimate. Hence there are 5-p and 6-p solutions at $G > 21$, and sources with 2-p solutions at $G \leq 21$ for which in principle a 5-p or 6-p solution was possible. See Lindegren et al. (2021b) for details on how the decision was taken to use the fall-back solution.

The three solution types can be identified through the `astrometric_params_solved` field in the *Gaia* EDR3 archive which equals 3, 31, and 95, respectively for 2-p, 5-p, and 6-p astrometric solutions. Fig. 2 shows the distribution of the three solution types over magnitude. We note the prevalence of 6-p solutions at $G < 4$ and the relative increase in 6-p solutions around $G = 11$. In both cases this reflects the source list evolution at these magnitudes, where for a large fraction of sources the change in source identifier (ID) prevented looking up the colour calculated for the corresponding source in *Gaia* DR2. The 100% fraction of sources with 2-p solutions at $G > 21$ is by construction (Lindegren et al. 2021b).

Along with the astrometry, new data quality indicators are published as part of *Gaia* EDR3. The renormalised unit weight error, introduced after *Gaia* DR2 was published (RUWE; Lindegren 2018)[2], is now part of the release. New quality indicators, related to the image parameter determination process, provide indications whether a source is one of a close pair (possibly a binary) or whether the data suffers from nearby disturbing sources. The indicators are as follows:

[1] https://gea.esac.esa.int/archive/documentation/GEDR3/index.html

[2] https://www.cosmos.esa.int/web/gaia/dr2-known-issues#AstrometryConsiderations

Table 3. Basic performance statistics for *Gaia* EDR3.

Data product or source type	Typical uncertainty
Five-parameter astrometry (position)	0.01–0.02 mas at $G < 15$
	0.05 mas at $G = 17$
	0.4 mas at $G = 20$
	1.0 mas at $G = 21$
Five-parameter astrometry (parallax)	0.02–0.03 mas at $G < 15$
	0.07 mas at $G = 17$
	0.5 mas at $G = 20$
	1.3 mas at $G = 21$
Five-parameter astrometry (proper motion)	0.02–0.03 mas yr^{-1} at $G < 15$
	0.07 mas yr^{-1} at $G = 17$
	0.5 mas yr^{-1} at $G = 20$
	1.4 mas yr^{-1} at $G = 21$
Six-parameter astrometry (position)	0.02–0.03 mas at $G < 15$
	0.08 mas at $G = 17$
	0.4 mas at $G = 20$
	1.0 mas at $G = 21$
Six-parameter astrometry (parallax)	0.02–0.04 mas at $G < 15$
	0.1 mas at $G = 17$
	0.5 mas at $G = 20$
	1.4 mas at $G = 21$
Six-parameter astrometry (proper motion)	0.02–0.04 mas yr^{-1} at $G < 15$
	0.1 mas yr^{-1} at $G = 17$
	0.6 mas yr^{-1} at $G = 20$
	1.5 mas yr^{-1} at $G = 21$
Two-parameter astrometry (position only)	1–3 mas
Systematic astrometric errors (averaged over the sky)	< 0.05 mas
Gaia-CRF3 alignment with ICRF	0.01 mas at $G = 19$
Gaia-CRF3 rotation with respect to ICRF	< 0.01 mas yr^{-1} at $G = 19$
Mean G-band photometry	0.3 mmag at $G < 13$
	1 mmag at $G = 17$
	6 mmag at $G = 20$
Mean G_{BP}-band photometry	0.9 mmag at $G < 13$
	12 mmag at $G = 17$
	108 mmag at $G = 20$
Mean G_{RP}-band photometry	0.6 mmag at $G < 13$
	6 mmag at $G = 17$
	52 mmag at $G = 20$

Notes. The astrometric uncertainties and the *Gaia*-CRF3 alignment and rotation limits refer to epoch J2016.0 TCB.

ipd_gof_harmonic_amplitude. This statistic measures the amplitude of the variation of the image parameter determination goodness of fit (reduced χ^2) as function of the position angle of the scan direction. A large amplitude indicates that the source is double, in which case the phase (next item) indicates the position angle of the pair, modulo 180 degrees.

ipd_gof_harmonic_phase. This statistic measures the phase of the variation of the IPD goodness of fit as function of the position angle of the scan direction

ipd_frac_multi_peak. This field provides information on the observation windows used for the astrometric processing of this source. It provides the fraction of windows for which the IPD algorithm has identified a double peak, meaning that the detection may be a resolved double star (either an optical pair or a physical binary).

ipd_frac_odd_win. Percentage of transits with truncated windows or multiple gates applied to a window. A high percentage indicates that a source is disturbed due to nearby sources in a crowded field or due to a nearby bright ($G < 13$) source.

The reference epoch for all sources is J2016.0 (TCB). This epoch near the middle of the observation interval included in *Gaia* EDR3 was chosen to minimise correlations between the position and proper motion parameters. This epoch is 0.5 year later than the reference epoch for *Gaia* DR2, which should be accounted for when comparing source positions between the two releases.

As in previous releases all sources were treated as single stars when solving for the astrometric parameters. For a binary the parameters may thus refer to either component, or to the photocentre of the system, and the proper motion represents the mean motion of the component, or photocentre, over the 2.8 years of

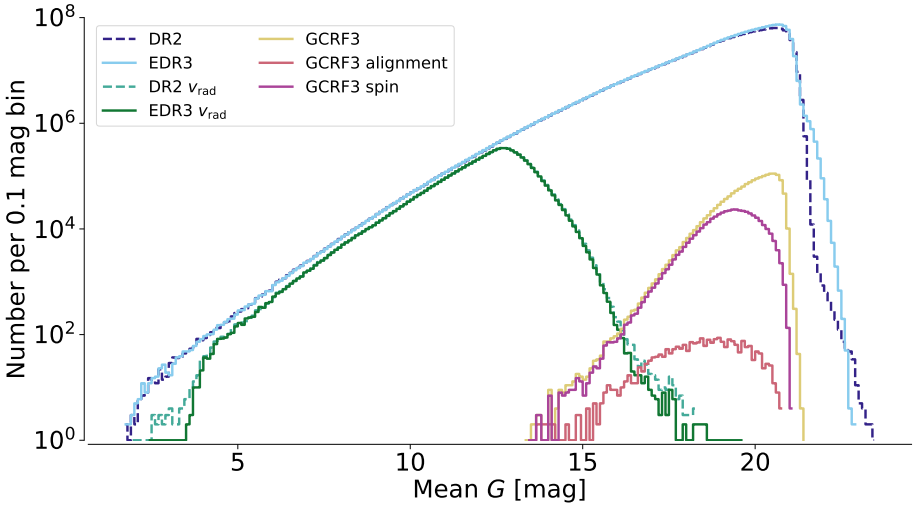


Fig. 1. Distribution of the mean values of G for all *Gaia* EDR3 sources shown as histograms with 0.1 mag wide bins. The distribution of the *Gaia* DR2 sources (dashed lines, for the full catalogue and for the radial velocity sample) is included for comparison. The other histograms are for the main *Gaia* EDR3 components as indicated in the legend.

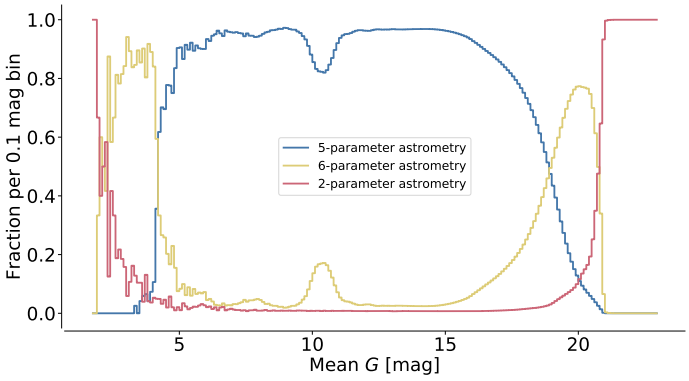


Fig. 2. Distribution of the fraction of astrometric solution types as a function of G-band magnitude.

data included in the solution. Depending on the orbital motion, this could be significantly different from the proper motion of the same object in *Gaia* DR2, and significantly different from the proper motion of the centre of mass of the binary.

The positions and proper motions are provided with respect to the third realisation of the *Gaia* celestial reference frame (*Gaia*-CRF3) which is aligned with the International Celestial Reference Frame (ICRF) to about 0.01 mas root-mean-square (RMS) at epoch J2016.0 (TCB), and non-rotating with respect to the ICRF to within 0.01 mas yr^{-1} RMS. The *Gaia*-CRF3 is materialised by 1 614 173 QSOs and aligned to the ICRF through a subset of 2269 QSOs. The construction and properties of the *Gaia*-CRF3 and the comparison to the ICRF are described in Gaia Collaboration et al. (2021b).

3.2. Photometric data set

The photometric data set contains the broad band photometry in the G, G_{BP}, and G_{RP} bands. The mean value of the G-band fluxes is reported for practically all sources while for about 85 per cent of the sources the mean values of the G_{BP} and G_{RP} fluxes are provided. For a small fraction of the sources any of the three bands may be missing (see Sect. 6.3.2). As for *Gaia* DR2, the photometric data processing consisted of three categories, "Gold", "Silver", and "Bronze", which represent decreasing quality levels of the photometric calibration achieved, where in the case of the Bronze sources no colour information is available. The photometric processing category of each source is indicated in the released catalogue by a numeric field (`phot_proc_mode`) assuming values 0, 1, and 2 for gold, silver, and bronze sources respectively. At the bright end the photometric uncertainties are dominated by calibration effects which are estimated to contribute 2.0, 3.1, and 1.8 mmag RMS per CCD observation, respectively for G, G_{BP}, and G_{RP} (Riello et al. 2021).

Two new data quality indicators are included with the photometry which allow filtering of sources according to the probability that their photometry is affected by crowding effects. The fields `phot_bp_n_blended_transits` and `phot_bp_n_contaminated_transits` (and similar for RP) indicate the number of transits for a given source believed to be affected by "blending" or "contamination". The former refers to the presence of another source in the same observation window or very nearby, and the latter refers to the presence of sources in the wider neighbourhood of the target source, which are bright enough to contribute flux to the observation window. The ratio between the numbers in these fields and the total number of transits (`phot_bp_n_obs` or `phot_rp_n_obs`) can be used to identify sources for which the photometry is possibly less reliable (see Riello et al. 2021, for a more detailed discussion).

3.3. Radial velocity data set

The radial velocity spectrograph data processing relies on the preliminary astrometric solution (AGIS-3.1 in Lindegren et al. 2021b) in order to have sufficiently accurate source positions to fix the correct wavelength scale of the RVS spectra. This means that the RVS processing can only start later during a processing cycle. In the planning of the *Gaia* EDR3 and *Gaia* DR3 releases it was not possible to accommodate the full sequence of RVS processing, radial velocity estimation, and validation, to allow new radial velocities to be published as part of *Gaia* EDR3. These will instead appear with *Gaia* DR3 in 2022. At the time of writing, the *Gaia* DR3 RVS processing is finished and the results are undergoing internal validation through the use of epoch radial velocities in the non-single star pipeline, and of RVS spectra in the astrophysical characterisation of *Gaia* sources.

In order to keep *Gaia* EDR3 maximally useful it was decided to copy *Gaia* DR2 radial velocities to this release. The evolution of the source list (Torra et al. 2021) necessitated a careful tracing of *Gaia* DR2 sources to their *Gaia* EDR3 counterparts, before assigning the DR2 radial velocities to the latter. The opportunity was used to also clean up the list of radial velocities from the potentially spurious values identified by Boubert et al. (2019).

The process is described in detail in Seabroke et al. (2021). The result is that 7 209 831 out of 7 224 631 *Gaia* DR2 radial velocities were transferred to *Gaia* EDR3, where 97% of the *Gaia* EDR3 sources with a radial velocity have the same source ID as in *Gaia* DR2. The radial velocities that were discarded correspond to sources that could not be traced to *Gaia* EDR3 or were shown, from a comparison with *Gaia* DR3 preliminary radial velocities and investigations of the raw observations, to have unreliable or erroneous radial velocities. The histograms presented in Seabroke et al. (2021) show that in particular in the tails of the distribution (at $|v_{\rm rad}| > 600$ km s^{-1}) radial velocities have been removed. It is also noteworthy that of the $\sim$ 70 000 potentially spurious radial velocities identified by Boubert et al. (2019), 96% were retained as reliable in *Gaia* EDR3. We note that all radial velocity related fields in the *Gaia* EDR3 archive are prefixed with "`dr2_`", leading to `dr2_radial_velocity`, `dr2_radial_velocity_error`, etc. For the detailed characteristics of the radial velocity data set (precision, accuracy, limitations) please refer to the relevant *Gaia* DR2 papers (Sartoretti et al. 2018; Katz et al. 2019; Gaia Collaboration et al. 2018).

The distribution of the astrometric, photometric, and radial velocity data sets in G is shown in Fig. 1, where for comparison the distribution for *Gaia* DR2 is also shown. We note the improved completeness at the faint end, at magnitudes close to $G = 21$. With respect to *Gaia* DR2 there are noticeably fewer radial velocities at $G > 15$ and at $G < 4$, the latter due to the source list evolution at the bright end. The distribution of the *Gaia*-CRF3 sources shows a sharp drop at $G = 21$ which reflects that only QSOs at $G < 21$ were used for the construction of the reference frame. The magnitude distribution is also shown for the *Gaia*-CRF3 sources used for ensuring that the spin of the reference frame is zero, and for the *Gaia*-CRF3 sources used for the alignment of the reference frame (2269 ICRF3 sources with counterparts in *Gaia* EDR3).

4. Scientific performance and potential of *Gaia* EDR3

Gaia EDR3 is accompanied by four papers that provide basic demonstrations of the scientific quality of the results included in this release. The following topics are treated. The *Gaia* EDR3 proper motions of quasars reveal a systematic pattern that can be ascribed to the acceleration of the solar system barycentre with respect to the rest frame of distant extragalactic sources. The value and direction of the acceleration can be determined from these data. That this measurement is now possible is testament to the much improved quality of the astrometry, in particular thanks to the suppression of systematic errors (Gaia Collaboration et al. 2021c). The *Gaia* catalogue of nearby stars presents and characterises a carefully selected sample of sources located within 100 pc from the sun (Gaia Collaboration et al. 2021e). A study of the Galactic anti-centre region illustrates the increased richness in phase space unveiled by the more precise *Gaia* EDR3 proper motions (Gaia Collaboration et al. 2021a). The structure and properties of the Magellanic Clouds are studied in Gaia Collaboration et al. (2021d).

We note in the following a couple of specific areas of improvement in the *Gaia* EDR3 astrometry and photometry compared to *Gaia* DR2. For further insights into the increased data quality see Fabricius et al. (2021) and the papers cited above.

The overall completeness of the catalogue at the faint end has increased somewhat as can be appreciated from Fig. 1. At the bright end *Gaia* EDR3 has a similar level of incompleteness as *Gaia* DR2. The spatial resolution of *Gaia* EDR3 has slightly improved with respect to *Gaia* DR2. This can be seen from the number counts of source pairs as a function of their separation presented in Fabricius et al. (2021). The counts drop below the expected line for a random source distribution at $\sim$ 1.5 arcsec (2.2 arcsec for *Gaia* DR2). The improved resolution can also be seen in the increased completeness of visual pairs from the Washington Double Star catalogue (Fabricius et al. 2021). The completeness in close source pairs decreases rapidly below about 0.7 arcsec which is to be expected as the treatment of sources in crowded fields has not fundamentally changed between *Gaia* DR2 and *Gaia* EDR3, even if the crowding effects were better characterised during the data processing.

The better treatment of high proper motion stars at the source list creation stage and the generally cleaner source list has led to a much more reliable sample of high proper motion stars in *Gaia* EDR3. This is demonstrated in Fabricius et al. (2021) where the diagram of proper motion vs. parallax shows a striking improvement from *Gaia* DR2 to *Gaia* EDR3, with most of the high proper motion stars now located on the positive parallax side of the 500 km s^{-1} tangential velocity locus. The suppression of spurious parallaxes has also removed a lot of unrealistically high proper motions for stars with negative parallaxes.

5. Changes from *Gaia* DR2 to *Gaia* EDR3

In Gaia Collaboration et al. (2018) it was emphasised that *Gaia* DR2 should be treated as independent from *Gaia* DR1 due to the evolution of the source list and the photometric system. This still holds when using *Gaia* EDR3 instead of *Gaia* DR2, the two releases should be treated as independent and in particular the user of the data is warned against making source by source comparisons between the two releases. Comparison should only be done at the statistical level for well defined samples of sources.

We repeat here the change in reference epoch from J2015.5 for *Gaia* DR2 to J2016.0 for *Gaia* EDR3, which should be taken into account when propagating *Gaia* EDR3 source positions into the future or past. The photometric system has changed in terms of the better internal calibration leading to much smaller magnitude and colour terms, and a new set of passbands is presented in Riello et al. (2021). Synthetic photometry for the prediction of *Gaia* observations should be updated with the new passbands.

As stressed in Torra et al. (2021) the source lists of the *Gaia* data releases should be treated as completely independent. Although extensive efforts are made to ensure that a physical source retains its identifier across releases, changes in the identifier associated to a source will occur in a small fraction of cases. Ideally, a given *Gaia* DR2 source with its associated transits appears in *Gaia* EDR3 (and *Gaia* DR3) with the same source ID and the same transits, plus the new transits added for *Gaia* EDR3. This would allow a simple matching of the sources across the two releases through the source ID. However, for the reasons mentioned in Sect. 2.1 (and elaborated in Torra et al. 2021), this should *not* be done, instead the DR2 to DR3 match table in the *Gaia* archive (`dr2_neighbourhood`) should be used to trace sources from *Gaia* DR2 to *Gaia* EDR3. This prevents mistakes in cross-identifications of sources due to the source list evolution.

Another form of source list evolution is in the transits assigned to a given source ID. For a small fraction of sources a significant fraction of the transits that were assigned to the source for *Gaia* DR2 may have been reassigned to other sources or discarded altogether. This means that the source character may

change from *Gaia* DR2 to *Gaia* EDR3. The *Gaia* EDR3 archive contains the following fields to help in understanding why a source with the same source ID in *Gaia* DR2 and *Gaia* EDR3 may have significantly different source parameters (astrometry, photometry, etc):

matched_transits The total number of field of view transits m matched to a given source ID.
new_matched_transits The number of transits n newly included in the transit list of an existing source ID.
matched_transits_removed The number of transits r removed from the transit list of an existing source ID.

The fraction of transits retained for a source ID from *Gaia* DR2 to *Gaia* EDR3 is given by $(m-n)/(m-n+r)$. Fig. 15 in Torra et al. (2021) shows this fraction as a function of G-band magnitude, which is lower than 100% for a significant number of source IDs at $G \lesssim 12$ and $G \gtrsim 19$. For source IDs with large changes in the transit list one should be careful when making comparisons between *Gaia* DR2 and *Gaia* EDR3.

As an example we look a bit more closely at the 2179 sources for which the G-band magnitude in *Gaia* DR2 is less than 5. These can be traced to *Gaia* EDR3 with the following Astronomical Data Query Language (ADQL) query in the *Gaia* archive:

```
select dr2.source_id, dr2.phot_g_mean_mag,
    edr3.*
from gaiadr2.gaia_source as dr2
join gaiaedr3.dr2_neighbourhood as edr3
on dr2.source_id=edr3.dr2_source_id
where dr2.phot_g_mean_mag<5
order by dr2.source_id asc
```

This results in a list of 2208 matches from a *Gaia* DR2 to a *Gaia* EDR3 source. In 34 cases there are two possible matches in *Gaia* EDR3 for the *Gaia* DR2 source, where in all such cases one of the matches is rather far (> 0.9 arcsec) from the target position. This leaves 2174 "best" matches for very bright *Gaia* DR2 sources in *Gaia* EDR3, hence 5 sources in *Gaia* DR2 at $G_{\rm DR2} < 5$ have no counterpart in *Gaia* EDR3. Of the matched sources about 40% changed source ID, among which a prominent example is β Pictoris (*Gaia* DR2 4792774797545105664 → *Gaia* EDR3 4792774797545800832).

These drastic changes occur mostly at the bright end as shown in Fig. 1 in Fabricius et al. (2021). For all other magnitudes the changes in source ID occur for a few per cent of the sources, except over the range $9 < G < 12$ where up to almost 10 per cent of the sources changed ID.

6. Using *Gaia* EDR3 data: Completeness and limitations

Gaia EDR3 represents a significant improvement in *Gaia* astrometry and broad-band photometry, but as pointed out in Rowell et al. (2021), Torra et al. (2021), Lindegren et al. (2021b), and Riello et al. (2021), there are still many improvements to be made to the data processing. This implies that there are limitations which should be kept in mind when using *Gaia* EDR3 data. Next, we describe how the data were filtered between the data processing and release publication stages and what the main limitations are that the user should be aware of.

6.1. Gaia EDR3: Validation and source filtering

For details on how the quality of the *Gaia* EDR3 data were assessed we refer to the astrometric and photometric processing papers (Lindegren et al. 2021b; Riello et al. 2021) for validation at the pipeline level, while a more global view of the data quality is provided in Fabricius et al. (2021). Here we describe the main filtering that was applied before accepting a source for publication.

6.1.1. Astrometry

The filtering of the astrometric data set was very similar to the procedure used for *Gaia* DR2. The results were filtered by requiring that a source was observed by *Gaia* at least five times (five focal plane transits), and that the semi-major axis of the position uncertainty ellipse is less than 100 mas. In contrast to *Gaia* DR2, no filtering on astrometric excess noise was done. The parallax and proper motions are determined only for sources satisfying the requirement that they are brighter than $G = 21$, the number of "visibility periods" used is at least 9 (a visibility period represents a group of observations separated from other such groups by at least four days), and the semi-major axis of the 5-dimensional uncertainty ellipse is below a magnitude dependent threshold. We refer to Lindegren et al. (2021b) for the details. For sources that do not meet these requirements only the positions are reported in *Gaia* EDR3. We remind the reader that the sources with parallaxes and proper motions fall into the two categories of 5-p and 6-p astrometry solutions (see Sect. 3.1). For source pairs closer together than 0.18 arcsec only one source was retained (detailed criteria in Lindegren et al. 2021b), which is then marked as a `duplicate_source` in the *Gaia* EDR3 archive.

6.1.2. Photometry

Unlike the previous releases, sources were not discarded from *Gaia* EDR3 if no G-band photometry was available. There are in fact some 5.5 million sources in *Gaia* EDR3 without a value for G in the published catalogue. For these sources the values of G could only be estimated after the processing and validation stages were finished and they will be provided through a separate channel (see Sect. 7.2). The criteria to publish photometry for a source are: the G-band is only provided for sources with `phot_g_n_obs` ≥ 10; the $G_{\rm BP}$-band is only provided for sources with `phot_bp_n_obs` ≥ 2; the $G_{\rm RP}$-band is only provided for sources with `phot_rp_n_obs` ≥ 2. We note that any of the photometric bands can be absent for a given source. No filtering on the flux excess factor was done (in contrast to *Gaia* DR2).

6.2. Survey completeness

Fig. 1 shows that the completeness of the *Gaia* survey has improved slightly with respect to *Gaia* DR2 at the faint end, between $G \approx 19$ and $G \approx 21$. The fraction of bright stars missing at $G < 7$ is unchanged with respect to *Gaia* DR2. The brightest star in *Gaia* EDR3 is at $G = 1.73$.

The large-scale completeness limit, as estimated by the 99th percentile of the G magnitude distribution (Fabricius et al. 2021), varies between $G \sim 20$ at low galactic latitudes ($b \lesssim 30$) and around the Magellanic Clouds, to $G \sim 22$ at higher latitudes. The survey limit variations over the sky show clear imprints of the *Gaia* scanning pattern.

In crowded regions the capability to observe all stars is reduced (Gaia Collaboration et al. 2016b). In combination with the still limited data treatment in crowded areas this means that the survey limit in regions with densities above a few hundred

thousand stars per square degree can be substantially brighter than $G = 20$. Fabricius et al. (2021) show that the completeness as measured on OGLE fields is 100% up to source densities of 2×10^5 deg^{-2}, while at higher densities the completeness has improved with respect to *Gaia* DR2, staying close to 100% up to 6×10^5 stars deg^{-2} and dropping to 50% at densities over 8×10^5 deg^{-2}. Fabricius et al. (2021) also studied the completeness in a sample of 26 globular clusters which were observed previously with the Hubble Space Telescope. On average they find a completeness at $G = 17$ of $\sim$ 80% for densities below 5×10^5 stars deg^{-2}, $\sim$ 50% at 5×10^5–2×10^6 stars deg^{-2}, and $\sim$ 15% at 2×10^6–2×10^7 stars deg^{-2}, with strong variations across the clusters and between the cores and the outer regions. In the very densest regions the incompleteness can be so severe as to give the appearance of holes in the source distribution.

As described in Sect. 4, the effective angular resolution of the *Gaia* EDR3 source list has slightly improved with respect to *Gaia* DR2, with incompleteness in close pairs of stars starting below about 1.5 arcsec. Refer to Fabricius et al. (2021) for details. Fabricius et al. (2021) note that among the source pairs with separations between 0.18 and 0.4 arcseconds there may be many spurious solutions.

6.3. Limitations

6.3.1. Astrometry

The major gain in the precision of parallaxes and proper motions from *Gaia* DR2 to *Gaia* EDR3 is complemented by a significant reduction in the systematic errors, which is evident from the reduced variance in the parallax and proper motion bias variations over the sky, and confirmed by the beautiful measurement of the acceleration of the solar system barycentre with respect to the distant universe. Nevertheless the following characteristics of the astrometry should be kept in mind.

The two solution types, 5-parameter and 6-parameter, behave differently in terms of uncertainties and systematics, with the 6-p astrometry in general being less precise. For the 5-p solutions the astrometric uncertainties are underestimated by $\sim$ 5% at the faint end ($G > 16$) and by up to $\sim$ 30% at the bright end ($G < 14$). For the 6-p solutions the numbers are $\sim$ 20% and up to $\sim$ 40%, respectively. The underestimation of the uncertainties increases in crowded areas such as the Large Magellanic Cloud, and for sources with indications that they may have companions or be part of a partially resolved double. The details can be found in Fabricius et al. (2021).

By examining the distribution of negative parallaxes, Fabricius et al. (2021) estimate that among the sources with formally high quality parallaxes ($\varpi/\sigma_\varpi > 5$) some 1.6% of the 1.5 billion 5-p and 6-p astrometric solutions are spurious, meaning that the listed parallax may be significantly in error despite the formally high precision. Fabricius et al. (2021) show that the fraction of spurious solutions is strongly dependent on magnitude and source density on the sky. For faint sources ($G \gtrsim 17$ for 6-p astrometric solutions and $G \gtrsim 19$ for 5-p solutions) and in crowded regions the fractions of spurious solutions can reach 10 per cent or more. It should be stressed that the spurious astrometric solutions in *Gaia* EDR3 produce smaller errors on the astrometric parameters than was the case for *Gaia* DR2.

The global parallax zero point for *Gaia* EDR3, as measured from quasars, is -17 μas. The RMS angular (i.e. source to source) covariances of the parallaxes and proper motions on small scales are $\sim$ 26 μas and $\sim$ 33 μas yr^{-1}, respectively. Details on the angular covariances can be found in Lindegren et al. (2021b). The parallax zero point (and the proper motion systematics) varies as a function of magnitude, colour, and celestial position. This is described in detail in Lindegren et al. (2021a).

6.3.2. Photometry

The increased precision and homogeneity of the *Gaia* EDR3 broad band photometry make it harder to assess the external accuracy of the photometry. Nevertheless Riello et al. (2021) show that the discontinuities that appeared at $G = 13$ and $G = 16$, when comparing the *Gaia* DR2 photometry to APASS (Henden et al. 2015, 2016) and SDSS DR15 (Aguado et al. 2019), have disappeared in *Gaia* EDR3. As shown in Fabricius et al. (2021), the same is true of the strong saturation effects in G at the bright end, and the significant variation of the G-band zero point with magnitude present in *Gaia* DR2. The effects are now below the 0.01 magnitude level for most sources. We stress again that a single passband now suffices for all three bands, G, $G_{\rm BP}$, and $G_{\rm RP}$. The following issues with the photometry were revealed following internal investigations, all described in detail in Riello et al. (2021) and Fabricius et al. (2021).

For faint red sources the flux in the BP band is overestimated which leads to these sources appearing much bluer in ($G_{\rm BP} - G_{\rm RP}$) than they should be. This can be recognised for example in open cluster colour magnitude diagrams as a blue-ward turn of the lower main sequence in G vs. ($G_{\rm BP} - G_{\rm RP}$). This issue is caused by the rejection of observations with G-band fluxes below 1 e$^-$ s^{-1}, where the rejection was also applied to the BP and RP observations. This does not cause problems for G and $G_{\rm RP}$, but at the faint end leads to overestimated BP fluxes.

During the internal validation of the *Gaia* EDR3 photometry a small tail of sources going as faint as $G \approx 25.5$ was noticed. Such faint sources will never be observed by *Gaia*, even when taking into account the fuzziness of the nominal $G = 20.7$ survey limit. The problem was traced to sources with unreliable colours for which the application of the internal photometric calibration failed (Riello et al. 2021; Fabricius et al. 2021). As a result it was decided to remove from the *Gaia* EDR3 catalogue the unreliable fluxes and magnitudes, which means there are sources for which any of the three bands could be missing. All in all there are 5 455 339 sources for which no G-band flux is available in the main *Gaia* EDR3 catalogue. For these sources the G-band flux was estimated ad-hoc by calibrating the sources assuming default colours. The values are available as a separate table through the *Gaia* EDR3 "known issues" pages[3]. For 54 125 of the sources without G-band fluxes this ad-hoc calibration was not possible. An indication of their brightness will be provided based on the on-board magnitude estimate.

At the image parameter determination stage (which precedes the astrometric and photometric data processing) the G-band fluxes (and locations) of sources for which no reliable colour information was available (from *Gaia* DR2) were estimated with a PSF or LSF model for a default source colour. This concerns the sources for which in the astrometry 6-p solutions were derived, which mitigated the remaining chromatic effect in the source image locations, as well as sources with 2-p solutions. Such a colour effect is also present in the fluxes but this was unfortunately not accounted for in the photometric processing. However, it is possible to correct the published G-band photometry for sources with 6-p solutions (`astrometric_params_solved = 95`) to bring

[3] https://www.cosmos.esa.int/web/gaia/edr3-known-issues

them onto the photometric system of the 5-p sources. The correction formula is presented in Riello et al. (2021) and should also be applied to sources with 2-p astrometric solutions (`astrometric_params_solved` = 3). We stress that this issue is *not* related to the photometric pass-bands.

For bright and extremely blue sources ($G < 13$, $G_{\rm BP} - G_{\rm RP} < -0.1$) there is a residual trend of about 5 mmag/mag for sources in the range $8 < G < 13$, when comparing the *Gaia* EDR3 magnitudes to synthetic magnitudes derived from BP and RP spectra. This is only seen in G and is probably related to deficiencies in the PSF modelling for bright stars. At $G < 8$ the residuals are dominated by saturation effects.

7. Using *Gaia* EDR3 data: Additional guidance

Here we provide some further advice on the use of the *Gaia* EDR3 data. This concerns issues specific to this release. The papers listed in Sect. 4 provide extensive examples of how to use *Gaia* EDR3 data responsibly, and we remind the reader of the need to be careful when estimating distances from parallaxes with relatively large uncertainties (Luri et al. 2018). We note again, as stressed in Sect. 5, that tracing sources from *Gaia* DR2 to *Gaia* EDR3 should not be done by blindly matching source IDs. The *Gaia* DR2 to *Gaia* EDR3 match table (`dr2_neighbourhood`) should be used for this purpose.

7.1. Astrometry

Fabricius et al. (2021) make the following recommendation for dealing with spurious astrometric solutions. Even when selecting only a sample of high-quality parallaxes, for example $\varpi/\sigma_\varpi > 5$, one should select also the corresponding sample with negative parallaxes ($\varpi/\sigma_\varpi < -5$) in order to ascertain what fraction of the positive parallaxes may in fact be spurious. The parameter `ipd_gof_harmonic_amplitude` is useful in identifying spurious solutions as shown in Fabricius et al. (2021), where values above 0.1 in combination with a `ruwe` larger than 1.4 are indicative of resolved doubles, which are still not correctly handled in the astrometric processing, and may cause spurious solutions.

For the sources with 6-p solutions there will in many cases be independent colour information available from photometric or spectroscopic observations, which may provide a superior estimate for $\nu_{\rm eff}$ than the value estimated during the *Gaia* EDR3 astrometric data processing. In these cases it is possible to incorporate the better colour information to update the astrometry for the 6-p solution to more precise values. The formulae for calculating the updated astrometry are given in the appendix of Lindegren et al. (2021b), where it is demonstrated that for significant correlations (coefficients larger than 0.3) between the pseudo-colour and the astrometric parameters, real gains in precision and accuracy can be expected.

Lindegren et al. (2021a) present an extensive investigation of the parallax zero point variations as a function of source brightness, colour, and celestial position. The samples used in this investigation are quasars, the Large Magellanic Cloud, red clump stars – sources for which the parallax is precisely known from independent estimates – and wide pairs of co-moving stars for which the parallaxes should be the same. As a result of the detailed characterisation of the zero point variations, a correction recipe is presented, separately for sources with 5-p and 6-p astrometry, which allows removing the parallax bias as a function of source magnitude, colour, and ecliptic latitude. It should be stressed that this is a tentative recipe, primarily intended as an illustration of how corrections could be derived for other samples of sources for which precise independent distance information is available. The recipe is not intended to be applied blindly and has not been applied to the published *Gaia* EDR3 parallaxes. Python code to apply the recipe will be made available as part of the *Gaia* EDR3 access facilities[4].

7.2. Photometry

Riello et al. (2021) provide guidance on the use of the *Gaia* EDR3 photometry which we summarise here. Further insights into the photometric data are presented by Fabricius et al. (2021).

The $G_{\rm BP}$ flux of faint sources is likely to be biased (Sect. 6.3.2) and one can elect to filter on the value of $G_{\rm BP}$, retaining only the brighter bias-free sources. This introduces undesirable selection effects and a better alternative may be to use the $(G - G_{\rm RP})$ colour, for example when studying the lower main sequence.

The G-band photometry for sources with 2-p or 6-p astrometric solutions should be corrected to account for the use of a default colour at the flux estimation stage, the correction formula is presented in Riello et al. (2021). In Appendix A we show how to calculate the corrections on the fly as part of a *Gaia* EDR3 archive query, and also present Python code that can be used for the same purpose. We note that out of the 344 million 2-p sources present in *Gaia* EDR3, about 20 million have an astrometric solution in which the actual source colour was used instead of a default colour. This means that for these 20 million 2-p sources the G-band correction should actually not be applied. These sources are mostly faint, with 96% at magnitudes $G > 20$, and for 75% of these 20 million sources the correction that is (wrongly) applied amounts to less than 4 milli-magnitudes. It was thus decided not to make a special effort to exclude these sources from the correction recipe presented in Appendix A. Should a user of the *Gaia* EDR3 data wish to undo the wrong correction for one or more of these 20 million sources, the list of source IDs and applied corrections can be provided on request.

For sources where the G magnitude is missing, the value can be looked up in separate tables to be provided through the *Gaia* EDR3 "known issues" web pages. While this may seem unnecessarily cumbersome, this choice was deliberately made to ensure that it is very clear to the user that the G-band magnitudes for these sources are from a very different origin (from an ad-hoc calibration, and for a small number of sources from the on-board magnitude estimate) and not directly comparable to the main catalogue photometry.

As was the case for *Gaia* DR2, at the bright end ($G < 8$ for G and $G \lesssim 4$ for $G_{\rm BP}$ and $G_{\rm RP}$) the magnitudes should be corrected for saturation effects. The correction formulae can be found in the appendix of Riello et al. (2021).

An important point made in Riello et al. (2021) is that the flux excess factor in *Gaia* EDR3 is much more representative of astrophysical inconsistencies between the fluxes in BP and RP with respect to the flux in G, for example due to the extended nature of a source or its non-standard (non-stellar) spectral energy distribution (although Fabricius et al. (2021) show that some artefacts in the photometry can still be traced in the flux excess factor). It is thus not possible to easily identify problematic photometry through the flux excess factor, and using this quantity in the construction of samples should be done with care. Refer to Riello et al. (2021) for detailed guidance. They present a corrected version of the flux excess factor which is recommended

[4] https://gitlab.com/icc-ub/public/gaiadr3_zeropoint

for use instead of the raw `phot_bp_rp_excess_factor` value listed in *Gaia* EDR3. The corrected version can be calculated from the formula presented in section 6 of Riello et al. (2021). Appendix B shows how to include the correction of the flux excess factor within an ADQL query, and presents Python code to achieve the same.

As described in Sect. 3.2, *Gaia* EDR3 contains fields from which a metric can be constructed that indicates how likely it is that the photometry of a given source is affected by crowding. This metric should be used with some care, which is explained further in Riello et al. (2021).

Finally, due to the evolution of the source list and the improvements in the photometry we strongly discourage comparisons between *Gaia* EDR3 and *Gaia* DR2 photometry, in particular on a source by source basis. Comparisons at the sample level are likely to reveal mostly differences due to changes in the photometric system and errors in *Gaia* DR2.

8. *Gaia* EDR3 access facilities

The *Gaia* EDR3 data will be available through the archive hosted by ESA[5], with the facilities as described in Gaia Collaboration et al. (2016a) and Gaia Collaboration et al. (2018). The data is also accessible at the partner and affiliated data centres in Europe, the United States, Japan, Australia, and South Africa. These data centres provide their own access facilities, but do not necessarily host all data contained in the ESA *Gaia* archive. We note the following enhancements and changes.

The pointing of the *Gaia* telescopes as a function of time is available as the table `commanded_scan_law`. The pointing for the entire 34 month period covering *Gaia* EDR3 is available at 10 second intervals, and allows one to reconstruct how often and at what scan angles a given position on the sky was observed by *Gaia*. We note that the *commanded* pointing is provided which may deviate from the actual attitude of *Gaia* by up to 30 arcsec. In addition gaps in the data collection due to spacecraft or on-ground problems are not accounted for.

The *Gaia* Universe Model Snapshot (GUMS, Robin et al. 2012) and the corresponding simulated *Gaia* catalogue (GOG, Luri et al. 2014) are now available as part of the *Gaia* EDR3 archive in the tables `gaia_universe_model` and `gaia_source_simulation`, respectively. They correspond to version 20 of GUMS and GOG and are described in detail in the on-line documentation [6]. We note that a few issues in the simulations could not be corrected on time. Notably, young star kinematics were wrongly set, such that their astrometry should be corrected by the user before using the simulation. Essentially, the stars with ages less than 0.15 Gyr should follow the Milky Way rotation curve, while they do not (their mean rotation velocity was erroneously set to 0). In addition, RR Lyrae stars are missing from GUMS, and the number of outliers in GOG, both in astrometry and photometry, is larger than expected from the simulated errors.

The astrometric performance predictions for *Gaia* DR4 and beyond have been updated, based on an extrapolation of the *Gaia* EDR3 performance. The new predictions will appear on the *Gaia* science performance pages[7]. The tables `agn_cross_id` and `frame_rotator_source` provide the source IDs of the *Gaia*-CRF3 sources.

Pre-computed cross matches to other large surveys are provided. We recommend using these cross-matches because they have been carefully validated and their use facilitates reproducing analyses of *Gaia* EDR3 data combined with other survey data. The details of the cross-match procedure are provided in Marrese et al. (2021) (see also Marrese et al. 2017, 2019). Pre-computed cross-matches are provided for the following surveys: Hipparcos (new reduction, van Leeuwen 2007); *Tycho*-2 (Høg et al. 2000), merged with the Tycho Double Star Catalogue (Fabricius et al. 2002); 2MASS (point source and extended catalogue merged, Skrutskie et al. 2006); SDSS DR13 (Albareti et al. 2017); Pan-STARRS1 (Chambers et al. 2016); SkyMapper DR2 (Onken et al. 2019); AllWise (Wright et al. 2010); URAT1 (Zacharias et al. 2015); GSC2.3 (Lasker et al. 2008); APASS DR9 (Henden et al. 2016, 2015); and RAVE DR5 (Kunder et al. 2017).

9. Conclusions

Gaia EDR3 represents another significant advance in the series of data releases resulting from the *Gaia* mission. Based on 34 months of input data, this release features major improvements in the astrometry and broad-band photometry, where for the first time the astrometry and photometry benefit from iterative processing between the determination of image locations and fluxes, and the astrometric solution. Other significant improvements are the increased robustness and stability of the source list and a much more sophisticated modelling of the PSF and LSF for the astrometric instrument. Next to the significant increase in the precision of the astrometry and photometry, the suppression of systematic errors is a major component of the improvements.

Gaia EDR3 represents the first installment of the *Gaia* DR3 release planned for publication in 2022. *Gaia* DR3 will feature new data products of which the BP, RP, and RVS spectra (to be released for a subset of sources) and the non-single star catalogue represent qualitative changes in character with respect to *Gaia* DR2. The planned contents are: astrometry and broad-band photometry from *Gaia* EDR3 will remain unchanged for *Gaia* DR3, and the same is true for the source list; an expanded radial velocity survey (some 30 million stars brighter than $G_{\rm RVS} \sim 14$); astrophysical parameter estimates based on the parallaxes, broad-band photometry, and BP, RP, and RVS spectra, where the latter are a new element enabling a richer astrophysical characterisation of sources; an order of magnitude larger sample of variable stars, with their light curves, classifications, and astrophysical properties; a non-single star (mostly binary stars) catalogue based on the analysis of epoch astrometry, epoch radial velocities and the light curves of eclipsing binaries; analyses of extended objects (galaxies, and QSO hosts); epoch astrometry and photometry, as well as orbits, for an expanded list of over 100 000 solar system objects; mean BP, RP, and RVS spectra, for a subset of astrophysically well-characterised sources; reflectance spectra for $\sim$ 5000 asteroids derived from BP and RP spectra; the *Gaia* Andromeda Photometric Survey (GAPS), which consists of the broad-band photometric time-series for *all* sources in a 5.5° radius field centred on M31.

There is thus much to look forward to in *Gaia* DR3, with the GAPS data set providing a taste of what is to come in *Gaia* DR4. We stress that epoch astrometry and epoch radial velocities will *not* appear in *Gaia* DR3 (except for solar system object epoch astrometry).

[5] https://archives.esac.esa.int/gaia
[6] https://gea.esac.esa.int/archive/documentation/GEDR3/Data_processing/chap_simulated/
[7] https://www.cosmos.esa.int/web/gaia/science-performance

Looking ahead, the *Gaia* spacecraft is currently in good overall health. The spacecraft operations since the appearance of *Gaia* DR2 have largely been smooth, with little to no degradation of the detectors in *Gaia*'s focal plane, except for the steadily increasing radiation damage. The latter is however still well below the anticipated levels before the launch of *Gaia*. The last decontamination of the telescopes and focal plane took place in August 2016 and no further decontamination was needed since. The current evolution of the throughput of the telescopes suggests that also in the future no further decontamination is needed. The only limiting factor to the lifetime of *Gaia* as a high precision astrometry mission is the amount of propellant for the micro-propulsion system. This is predicted to be exhausted in early 2025, after which time the attitude and spin rate of *Gaia* can no longer be maintained at the levels of precision needed for the astrometry. With this end-of-life date for *Gaia* in mind, and the end of the nominal mission planned for mid-2019, the process of applying for an extended mission was started already in 2016. The nominal *Gaia* mission ended on July 16, 2019 and *Gaia* has been in extended mission operations since that date. The mission extension is formally approved to the end of 2022 at the time of writing, with good hopes of the mission continuing to its estimated end-of-life. This would bring the total mission lifetime to 10 years, implying a 40 per cent improvement on the precision of all data products with respect to a five year mission, and a factor of almost three improvement for the proper motions.

In this context the community can look forward to two major data releases, *Gaia* DR4 and *Gaia* DR5, both incorporating data from the extended *Gaia* mission. *Gaia* DR4 will be based on 66 months of input data (which is already in hand), while *Gaia* DR5 will include all data collected over the entire (nominal + extended) *Gaia* mission. The extra half year of data from the extended mission included in the *Gaia* DR4 data processing is motivated by the wish to include part of the one year period between July 16, 2019 and July 29, 2020 when *Gaia* was operated with a reversed direction of the precession of the spin axis around the direction to the sun. This was introduced to break the degeneracy between the across-scan rate at which sources move across the focal plane and their parallax factor (see appendix B in Lindegren et al. 2021b, for more details). Including the first 6 months of the reverse precession period in the inputs for *Gaia* DR4 is expected to already significantly mitigate the effects of this degeneracy.

The main new features of *Gaia* DR4 are the publication of a list of exoplanets discovered with *Gaia* and the publication of all the time series data, meaning epoch astrometry, broad-band photometry, radial velocities, as well as BP, RP, and RVS spectra for *all* sources. This will be a significant expansion in the volume of data released. We leave to the imagination of the reader the expanded scientific possibilities.

Acknowledgements. This work presents results from the European Space Agency (ESA) space mission *Gaia*. *Gaia* data are being processed by the *Gaia* Data Processing and Analysis Consortium (DPAC). Funding for the DPAC is provided by national institutions, in particular the institutions participating in the *Gaia* MultiLateral Agreement (MLA). The *Gaia* mission website is https://www.cosmos.esa.int/gaia. The *Gaia* archive website is https://archives.esac.esa.int/gaia. The *Gaia* mission and data processing have financially been supported by, in alphabetical order by country: the Algerian Centre de Recherche en Astronomie, Astrophysique et Géophysique of Bouzareah Observatory; the Austrian Fonds zur Förderung der wissenschaftlichen Forschung (FWF) Hertha Firnberg Programme through grants T359, P20046, and P23737; the BELgian federal Science Policy Office (BELSPO) through various PROgramme de Développement d'Expériences scientifiques (PRODEX) grants and the Polish Academy of Sciences - Fonds Wetenschappelijk Onderzoek through grant VS.091.16N, and the Fonds de la Recherche Scientifique (FNRS); the Brazil-France exchange programmes Fundação de Amparo à Pesquisa do Estado de São Paulo (FAPESP) and Coordenação de Aperfeicoamento de Pessoal de Nível Superior (CAPES) - Comité Français d'Evaluation de la Coopération Universitaire et Scientifique avec le Brésil (COFECUB); the National Science Foundation of China (NSFC) through grants 11573054 and 11703065 and the China Scholarship Council through grant 201806040200; the Tenure Track Pilot Programme of the Croatian Science Foundation and the École Polytechnique Fédérale de Lausanne and the project TTP-2018-07-1171 'Mining the Variable Sky', with the funds of the Croatian-Swiss Research Programme; the Czech-Republic Ministry of Education, Youth, and Sports through grant LG 15010 and INTER-EXCELLENCE grant LTAUSA18093, and the Czech Space Office through ESA PECS contract 98058; the Danish Ministry of Science; the Estonian Ministry of Education and Research through grant IUT40-1; the European Commission's Sixth Framework Programme through the European Leadership in Space Astrometry (ELSA) Marie Curie Research Training Network (MRTN-CT-2006-033481), through Marie Curie project PIOF-GA-2009-255267 (Space AsteroSeismology & RR Lyrae stars, SAS-RRL), and through a Marie Curie Transfer-of-Knowledge (ToK) fellowship (MTKD-CT-2004-014188); the European Commission's Seventh Framework Programme through grant FP7-606740 (FP7-SPACE-2013-1) for the *Gaia* European Network for Improved data User Services (GENIUS) and through grant 264895 for the *Gaia* Research for European Astronomy Training (GREAT-ITN) network; the European Research Council (ERC) through grants 320360 and 647208 and through the European Union's Horizon 2020 research and innovation and excellent science programmes through Marie Skłodowska-Curie grant 745617 as well as grants 670519 (Mixing and Angular Momentum tranSport of massIvE stars – MAMSIE), 687378 (Small Bodies: Near and Far), 682115 (Using the Magellanic Clouds to Understand the Interaction of Galaxies), and 695099 (A sub-percent distance scale from binaries and Cepheids – CepBin); the European Science Foundation (ESF), in the framework of the *Gaia* Research for European Astronomy Training Research Network Programme (GREAT-ESF); the European Space Agency (ESA) in the framework of the *Gaia* project, through the Plan for European Cooperating States (PECS) programme through grants for Slovenia, through contracts C98090 and 4000106398/12/NL/KML for Hungary, and through contract 4000115263/15/NL/IB for Germany; the Academy of Finland and the Magnus Ehrnrooth Foundation; the French Centre National d'Etudes Spatiales (CNES), the Agence Nationale de la Recherche (ANR) through grant ANR-10-IDEX-0001-02 for the 'Investissements d'avenir' programme, through grant ANR-15-CE31-0007 for project 'Modelling the Milky Way in the Gaia era' (MOD4Gaia), through grant ANR-14-CE33-0014-01 for project 'The Milky Way disc formation in the Gaia era' (ARCHEOGAL), and through grant ANR-15-CE31-0012-01 for project 'Unlocking the potential of Cepheids as primary distance calibrators' (UnlockCepheids), the Centre National de la Recherche Scientifique (CNRS) and its SNO Gaia of the Institut des Sciences de l'Univers (INSU), the 'Action Fédératrice Gaia' of the Observatoire de Paris, the Région de Franche-Comté, and the Programme National de Gravitation, Références, Astronomie, et Métrologie (GRAM) of CNRS/INSU with the Institut National Polytechnique (INP) and the Institut National de Physique nucléaire et de Physique des Particules (IN2P3) co-funded by CNES; the German Aerospace Agency (Deutsches Zentrum für Luft- und Raumfahrt e.V., DLR) through grants 50QG0501, 50QG0601, 50QG0602, 50QG0701, 50QG0901, 50QG1001, 50QG1101, 50QG1401, 50QG1402, 50QG1403, 50QG1404, and 50QG1904 and the Centre for Information Services and High Performance Computing (ZIH) at the Technische Universität (TU) Dresden for generous allocations of computer time; the Hungarian Academy of Sciences through the Lendület Programme grants LP2014-17 and LP2018-7 and through the Premium Postdoctoral Research Programme (L. Molnár), and the Hungarian National Research, Development, and Innovation Office (NKFIH) through grant KH_18-130405; the Science Foundation Ireland (SFI) through a Royal Society - SFI University Research Fellowship (M. Fraser); the Israel Science Foundation (ISF) through grant 848/16; the Agenzia Spaziale Italiana (ASI) through contracts I/037/08/0, I/058/10/0, 2014-025-R.0, 2014-025-R.1.2015, and 2018-24-HH.0 to the Italian Istituto Nazionale di Astrofisica (INAF), contract 2014-049-R.0/1/2 to INAF for the Space Science Data Centre (SSDC, formerly known as the ASI Science Data Center, ASDC), contracts I/008/10/0, 2013/030/I.0, 2013-030-I.0.1-2015, and 2016-17-I.0 to the Aerospace Logistics Technology Engineering Company (ALTEC S.p.A.), INAF, and the Italian Ministry of Education, University, and Research (Ministero dell'Istruzione, dell'Università e della Ricerca) through the Premiale project 'MIning The Cosmos Big Data and Innovative Italian Technology for Frontier Astrophysics and Cosmology' (MITiC); the Netherlands Organisation for Scientific Research (NWO) through grant NWO-M-614.061.414, through a VICI grant (A. Helmi), and through a Spinoza prize (A. Helmi), and the Netherlands Research School for Astronomy (NOVA); the Polish National Science Centre through HARMONIA grant 2018/06/M/ST9/00311, DAINA grant 2017/27/L/ST9/03221, and PRELUDIUM grant 2017/25/N/ST9/01253, and the Ministry of Science and Higher Education (MNiSW) through grant DIR/WK/2018/12; the Portugese Fundação para a Ciência e a Tecnologia (FCT) through grants SFRH/BPD/74697/2010 and

SFRH/BD/128840/2017 and the Strategic Programme UID/FIS/00099/2019 for CENTRA; the Slovenian Research Agency through grant P1-0188; the Spanish Ministry of Economy (MINECO/FEDER, UE) through grants ESP2016-80079-C2-1-R, ESP2016-80079-C2-2-R, RTI2018-095076-B-C21, RTI2018-095076-B-C22, BES-2016-078499, and BES-2017-083126 and the Juan de la Cierva formación 2015 grant FJCI-2015-2671, the Spanish Ministry of Education, Culture, and Sports through grant FPU16/03827, the Spanish Ministry of Science and Innovation (MICINN) through grant AYA2017-89841P for project 'Estudio de las propiedades de los fósiles estelares en el entorno del Grupo Local' and through grant TIN2015-65316-P for project 'Computación de Altas Prestaciones VII', the Severo Ochoa Centre of Excellence Programme of the Spanish Government through grant SEV2015-0493, the Institute of Cosmos Sciences University of Barcelona (ICCUB, Unidad de Excelencia 'María de Maeztu') through grants MDM-2014-0369 and CEX2019-000918-M, the University of Barcelona's official doctoral programme for the development of an R+D+i project through an Ajuts de Personal Investigador en Formació (APIF) grant, the Spanish Virtual Observatory through project AyA2017-84089, the Galician Regional Government, Xunta de Galicia, through grants ED431B-2018/42 and ED481A-2019/155, support received from the Centro de Investigación en Tecnologías de la Información y las Comunicaciones (CITIC) funded by the Xunta de Galicia, the Xunta de Galicia and the Centros Singulares de Investigación de Galicia for the period 2016-2019 through CITIC, the European Union through the European Regional Development Fund (ERDF) / Fondo Europeo de Desenvolvemento Rexional (FEDER) for the Galicia 2014-2020 Programme through grant ED431G-2019/01, the Red Española de Supercomputación (RES) computer resources at MareNostrum, the Barcelona Supercomputing Centre - Centro Nacional de Supercomputación (BSC-CNS) through activities AECT-2016-1-0006, AECT-2016-2-0013, AECT-2016-3-0011, and AECT-2017-1-0020, the Departament d'Innovació, Universitats i Empresa de la Generalitat de Catalunya through grant 2014-SGR-1051 for project 'Models de Programació i Entorns d'Execució Parallels' (MPEXPAR), and Ramon y Cajal Fellowship RYC2018-025968-I; the Swedish National Space Agency (SNSA/Rymdstyrelsen); the Swiss State Secretariat for Education, Research, and Innovation through the Mesures d'Accompagnement, the Swiss Activités Nationales Complémentaires, and the Swiss National Science Foundation; the United Kingdom Particle Physics and Astronomy Research Council (PPARC), the United Kingdom Science and Technology Facilities Council (STFC), and the United Kingdom Space Agency (UKSA) through the following grants to the University of Bristol, the University of Cambridge, the University of Edinburgh, the University of Leicester, the Mullard Space Sciences Laboratory of University College London, and the United Kingdom Rutherford Appleton Laboratory (RAL): PP/D006511/1, PP/D006546/1, PP/D006570/1, ST/I000852/1, ST/J005045/1, ST/K00056X/1, ST/K000209/1, ST/K000756/1, ST/L006561/1, ST/N000595/1, ST/N000641/1, ST/N000978/1, ST/N001117/1, ST/S000089/1, ST/S000976/1, ST/S001123/1, ST/S001948/1, ST/S002103/1, and ST/V000969/1. This work made use of the following software: Astropy, a community-developed core Python package for Astronomy (Astropy Collaboration et al. 2013, 2018, http://www.astropy.org), IPython (Pérez & Granger 2007, https://ipython.org/), Jupyter (https://jupyter.org/), Matplotlib (Hunter 2007, https://matplotlib.org), SciPy (Virtanen et al. 2020, https://www.scipy.org), NumPy (Harris et al. 2020, https://numpy.org), and TOPCAT (Taylor 2005, http://www.starlink.ac.uk/topcat/). This work has made use of NASA's Astrophysics Data System. We thank the referee, Andy Casey, for a careful reading of the manuscript.

References

Aguado, D. S., Ahumada, R., Almeida, A., et al. 2019, ApJS, 240, 23
Albareti, F. D., Allende Prieto, C., Almeida, A., et al. 2017, ApJS, 233, 25
Arenou, F., Luri, X., Babusiaux, C., et al. 2018, A&A, 616, A17
Astropy Collaboration, Price-Whelan, A. M., Sipőcz, B. M., et al. 2018, AJ, 156, 123
Astropy Collaboration, Robitaille, T. P., Tollerud, E. J., et al. 2013, A&A, 558, A33
Boubert, D., Strader, J., Aguado, D., et al. 2019, MNRAS, 486, 2618
Butkevich, A. G., Klioner, S. A., Lindegren, L., Hobbs, D., & van Leeuwen, F. 2017, A&A, 603, A45
Carrasco, J. M., Weiler, M., Jordi, C., et al. 2021, arXiv e-prints, arXiv:2106.01752
Chambers, K. C., Magnier, E. A., Metcalfe, N., et al. 2016, ArXiv e-prints [arXiv:1612.05560]
Cropper, M., Katz, D., Sartoretti, P., et al. 2018, A&A, 616, A5
De Angeli et al. 2021, A&A in prep.
Evans, D. W., Riello, M., De Angeli, F., et al. 2018, A&A, 616, A4
Fabricius, C., Høg, E., Makarov, V. V., et al. 2002, A&A, 384, 180
Fabricius, C., Luri, X., Arenou, F., et al. 2021, A&A, 649, A5
Gaia Collaboration, Antoja, T., McMillan, P. J., et al. 2021a, A&A, 649, A8
Gaia Collaboration, Brown, A. G. A., Vallenari, A., et al. 2018, A&A, 616, A1
Gaia Collaboration, Brown, A. G. A., Vallenari, A., et al. 2016a, A&A, 595, A2
Gaia Collaboration, Klioner, S., & et al. 2021b, A&A in prep.
Gaia Collaboration, Klioner, S. A., Mignard, F., et al. 2021c, A&A, 649, A9
Gaia Collaboration, Luri, X., Chemin, L., et al. 2021d, A&A, 649, A7
Gaia Collaboration, Prusti, T., de Bruijne, J. H. J., et al. 2016b, A&A, 595, A1
Gaia Collaboration, Smart, R. L., Sarro, L. M., et al. 2021e, A&A, 649, A6
Hambly, N. C., Cropper, M., Boudreault, S., et al. 2018, A&A, 616, A15
Harris, C. R., Millman, K. J., van der Walt, S. J., et al. 2020, Nature, 585, 357–362
Henden, A. A., Levine, S., Terrell, D., & Welch, D. L. 2015, in American Astronomical Society Meeting Abstracts, Vol. 225, American Astronomical Society Meeting Abstracts #225, 336.16
Henden, A. A., Templeton, M., Terrell, D., et al. 2016, VizieR Online Data Catalogue, 2336
Høg, E., Fabricius, C., Makarov, V. V., et al. 2000, A&A, 355, L27
Hunter, J. D. 2007, Computing in Science and Engineering, 9, 90
Katz, D., Sartoretti, P., Cropper, M., et al. 2019, A&A, 622, A205
Kunder, A., Kordopatis, G., Steinmetz, M., et al. 2017, AJ, 153, 75
Lasker, B. M., Lattanzi, M. G., McLean, B. J., et al. 2008, AJ, 136, 735
Lindegren, L. 2018, technical note GAIA-C3-TN-LU-LL-124
Lindegren, L. 2020a, A&A, 633, A1
Lindegren, L. 2020b, A&A, 637, C5
Lindegren, L., Bastian, U., Biermann, M., et al. 2021a, A&A, 649, A4
Lindegren, L., Hernández, J., Bombrun, A., et al. 2018, A&A, 616, A2
Lindegren, L., Klioner, S. A., Hernández, J., et al. 2021b, A&A, 649, A2
Lindegren, L., Lammers, U., Hobbs, D., et al. 2012, A&A, 538, A78
Luri, X., Brown, A. G. A., Sarro, L. M., et al. 2018, A&A, 616, A9
Luri, X., Palmer, M., Arenou, F., et al. 2014, A&A, 566, A119
Maíz Apellániz, J. & Weiler, M. 2018, A&A, 619, A180
Marrese, P. M., Marinoni, S., Fabrizio, M., & Altavilla, G. 2019, A&A, 621, A144
Marrese, P. M., Marinoni, S., Fabrizio, M., & Altavilla, G. 2021, A&A in prep.
Marrese, P. M., Marinoni, S., Fabrizio, M., & Giuffrida, G. 2017, A&A, 607, A105
Michalik, D., Lindegren, L., Hobbs, D., & Butkevich, A. G. 2015, A&A, 583, A68
Montegriffo et al. 2021, A&A in prep.
Onken, C. A., Wolf, C., Bessell, M. S., et al. 2019, PASA, 36, e033
Pancino, E., Altavilla, G., Marinoni, S., et al. 2012, MNRAS, 426, 1767
Pérez, F. & Granger, B. E. 2007, Computing in Science and Engineering, 9, 21
Riello, M., De Angeli, F., Evans, D. W., et al. 2021, A&A, 649, A3
Robin, A. C., Luri, X., Reylé, C., et al. 2012, A&A, 543, A100
Rowell, N., Davidson, M., Lindegren, L., et al. 2021, A&A, 649, A11
Sartoretti, P., Katz, D., Cropper, M., et al. 2018, A&A, 616, A6
Seabroke, G., Fabricius, C., Teyssier, D., et al. 2021, submitted to A&A
Skrutskie, M. F., Cutri, R. M., Stiening, R., et al. 2006, AJ, 131, 1163
Smart, R. L. & Nicastro, L. 2014, A&A, 570, A87
Taylor, M. B. 2005, in Astronomical Society of the Pacific Conference Series, Vol. 347, Astronomical Data Analysis Software and Systems XIV, ed. P. Shopbell, M. Britton, & R. Ebert, 29
Torra, F., Castañeda, J., Fabricius, C., et al. 2021, A&A, 649, A10
van Leeuwen, F. 2007, Hipparcos, the New Reduction of the Raw Data, Astrophysics and Space Science Library. Vol. 350 edn. (Springer)
Virtanen, P., Gommers, R., Oliphant, T. E., et al. 2020, Nature Methods, 17, 261
Wright, E. L., Eisenhardt, P. R. M., Mainzer, A. K., et al. 2010, AJ, 140, 1868
Zacharias, N., Finch, C., Subasavage, J., et al. 2015, AJ, 150, 101

[1] Leiden Observatory, Leiden University, Niels Bohrweg 2, 2333 CA Leiden, The Netherlands

[2] INAF - Osservatorio astronomico di Padova, Vicolo Osservatorio 5, 35122 Padova, Italy

[3] European Space Agency (ESA), European Space Research and Technology Centre (ESTEC), Keplerlaan 1, 2201AZ, Noordwijk, The Netherlands

[4] Univ. Grenoble Alpes, CNRS, IPAG, 38000 Grenoble, France

[5] GEPI, Observatoire de Paris, Université PSL, CNRS, 5 Place Jules Janssen, 92190 Meudon, France

[6] Astronomisches Rechen-Institut, Zentrum für Astronomie der Universität Heidelberg, Mönchhofstr. 12-14, 69120 Heidelberg, Germany

[7] Université Côte d'Azur, Observatoire de la Côte d'Azur, CNRS, Laboratoire Lagrange, Bd de l'Observatoire, CS 34229, 06304 Nice Cedex 4, France

[8] Institute of Astronomy, University of Cambridge, Madingley Road, Cambridge CB3 0HA, United Kingdom

[9] Department of Astronomy, University of Geneva, Chemin des Maillettes 51, 1290 Versoix, Switzerland

[10] Aurora Technology for European Space Agency (ESA), Camino bajo del Castillo, s/n, Urbanizacion Villafranca del Castillo, Villanueva de la Cañada, 28692 Madrid, Spain

[11] Institut de Ciències del Cosmos (ICCUB), Universitat de Barcelona (IEEC-UB), Martí i Franquès 1, 08028 Barcelona, Spain

[12] Lohrmann Observatory, Technische Universität Dresden, Mommsenstraße 13, 01062 Dresden, Germany

[13] European Space Agency (ESA), European Space Astronomy Centre (ESAC), Camino bajo del Castillo, s/n, Urbanizacion Villafranca del Castillo, Villanueva de la Cañada, 28692 Madrid, Spain

[14] Lund Observatory, Department of Astronomy and Theoretical Physics, Lund University, Box 43, 22100 Lund, Sweden

[15] CNES Centre Spatial de Toulouse, 18 avenue Edouard Belin, 31401 Toulouse Cedex 9, France

[16] Institut d'Astronomie et d'Astrophysique, Université Libre de Bruxelles CP 226, Boulevard du Triomphe, 1050 Brussels, Belgium

[17] F.R.S.-FNRS, Rue d'Egmont 5, 1000 Brussels, Belgium

[18] INAF - Osservatorio Astrofisico di Arcetri, Largo Enrico Fermi 5, 50125 Firenze, Italy

[19] Laboratoire d'astrophysique de Bordeaux, Univ. Bordeaux, CNRS, B18N, allée Geoffroy Saint-Hilaire, 33615 Pessac, France

[20] Max Planck Institute for Astronomy, Königstuhl 17, 69117 Heidelberg, Germany

[21] Mullard Space Science Laboratory, University College London, Holmbury St Mary, Dorking, Surrey RH5 6NT, United Kingdom

[22] INAF - Osservatorio Astrofisico di Torino, via Osservatorio 20, 10025 Pino Torinese (TO), Italy

[23] University of Turin, Department of Physics, Via Pietro Giuria 1, 10125 Torino, Italy

[24] INAF - Osservatorio di Astrofisica e Scienza dello Spazio di Bologna, via Piero Gobetti 93/3, 40129 Bologna, Italy

[25] DAPCOM for Institut de Ciències del Cosmos (ICCUB), Universitat de Barcelona (IEEC-UB), Martí i Franquès 1, 08028 Barcelona, Spain

[26] Royal Observatory of Belgium, Ringlaan 3, 1180 Brussels, Belgium

[27] ALTEC S.p.a, Corso Marche, 79,10146 Torino, Italy

[28] Department of Astronomy, University of Geneva, Chemin d'Ecogia 16, 1290 Versoix, Switzerland

[29] Sednai Sàrl, Geneva, Switzerland

[30] Gaia DPAC Project Office, ESAC, Camino bajo del Castillo, s/n, Urbanizacion Villafranca del Castillo, Villanueva de la Cañada, 28692 Madrid, Spain

[31] Telespazio Vega UK Ltd for European Space Agency (ESA), Camino bajo del Castillo, s/n, Urbanizacion Villafranca del Castillo, Villanueva de la Cañada, 28692 Madrid, Spain

[32] SYRTE, Observatoire de Paris, Université PSL, CNRS, Sorbonne Université, LNE, 61 avenue de l'Observatoire 75014 Paris, France

[33] National Observatory of Athens, I. Metaxa and Vas. Pavlou, Palaia Penteli, 15236 Athens, Greece

[34] IMCCE, Observatoire de Paris, Université PSL, CNRS, Sorbonne Université, Univ. Lille, 77 av. Denfert-Rochereau, 75014 Paris, France

[35] INAF - Osservatorio Astrofisico di Catania, via S. Sofia 78, 95123 Catania, Italy

[36] Serco Gestión de Negocios for European Space Agency (ESA), Camino bajo del Castillo, s/n, Urbanizacion Villafranca del Castillo, Villanueva de la Cañada, 28692 Madrid, Spain

[37] Institut d'Astrophysique et de Géophysique, Université de Liège, 19c, Allée du 6 Août, B-4000 Liège, Belgium

[38] CRAAG - Centre de Recherche en Astronomie, Astrophysique et Géophysique, Route de l'Observatoire Bp 63 Bouzareah 16340 Algiers, Algeria

[39] Institute for Astronomy, University of Edinburgh, Royal Observatory, Blackford Hill, Edinburgh EH9 3HJ, United Kingdom

[40] ATG Europe for European Space Agency (ESA), Camino bajo del Castillo, s/n, Urbanizacion Villafranca del Castillo, Villanueva de la Cañada, 28692 Madrid, Spain

[41] ETSE Telecomunicación, Universidade de Vigo, Campus Lagoas-Marcosende, 36310 Vigo, Galicia, Spain

[42] Université de Strasbourg, CNRS, Observatoire astronomique de Strasbourg, UMR 7550, 11 rue de l'Université, 67000 Strasbourg, France

[43] Kavli Institute for Cosmology Cambridge, Institute of Astronomy, Madingley Road, Cambridge, CB3 0HA

[44] Department of Astrophysics, Astronomy and Mechanics, National and Kapodistrian University of Athens, Panepistimiopolis, Zografos, 15783 Athens, Greece

[45] Observational Astrophysics, Division of Astronomy and Space Physics, Department of Physics and Astronomy, Uppsala University, Box 516, 751 20 Uppsala, Sweden

[46] Leibniz Institute for Astrophysics Potsdam (AIP), An der Sternwarte 16, 14482 Potsdam, Germany

[47] CENTRA, Faculdade de Ciências, Universidade de Lisboa, Edif. C8, Campo Grande, 1749-016 Lisboa, Portugal

[48] Department of Informatics, Donald Bren School of Information and Computer Sciences, University of California, 5019 Donald Bren

[63] CITIC - Department of Computer Science and Information Technologies, University of A Coruña, Campus de Elviña S/N, 15071, A Coruña, Spain
[64] Barcelona Supercomputing Center (BSC) - Centro Nacional de Supercomputación, c/ Jordi Girona 29, Ed. Nexus II, 08034 Barcelona, Spain
[65] University of Vienna, Department of Astrophysics, Türkenschanzstraße 17, A1180 Vienna, Austria
[66] European Southern Observatory, Karl-Schwarzschild-Str. 2, 85748 Garching, Germany
[67] Kapteyn Astronomical Institute, University of Groningen, Landleven 12, 9747 AD Groningen, The Netherlands
[68] School of Physics and Astronomy, University of Leicester, University Road, Leicester LE1 7RH, United Kingdom
[69] Center for Research and Exploration in Space Science and Technology, University of Maryland Baltimore County, 1000 Hilltop Circle, Baltimore MD, USA
[70] GSFC - Goddard Space Flight Center, Code 698, 8800 Greenbelt Rd, 20771 MD Greenbelt, United States
[71] EURIX S.r.l., Corso Vittorio Emanuele II 61, 10128, Torino, Italy
[72] Harvard-Smithsonian Center for Astrophysics, 60 Garden St., MS 15, Cambridge, MA 02138, USA
[73] HE Space Operations BV for European Space Agency (ESA), Camino bajo del Castillo, s/n, Urbanizacion Villafranca del Castillo, Villanueva de la Cañada, 28692 Madrid, Spain
[74] CAUP - Centro de Astrofisica da Universidade do Porto, Rua das Estrelas, Porto, Portugal
[75] SISSA - Scuola Internazionale Superiore di Studi Avanzati, via Bonomea 265, 34136 Trieste, Italy
[76] Telespazio for CNES Centre Spatial de Toulouse, 18 avenue Edouard Belin, 31401 Toulouse Cedex 9, France
[77] University of Turin, Department of Computer Sciences, Corso Svizzera 185, 10149 Torino, Italy
[78] Dpto. de Matemática Aplicada y Ciencias de la Computación, Univ. de Cantabria, ETS Ingenieros de Caminos, Canales y Puertos, Avda. de los Castros s/n, 39005 Santander, Spain
[79] Centro de Astronomía - CITEVA, Universidad de Antofagasta, Avenida Angamos 601, Antofagasta 1270300, Chile
[80] Vera C Rubin Observatory, 950 N. Cherry Avenue, Tucson, AZ 85719, USA
[81] Centre for Astrophysics Research, University of Hertfordshire, College Lane, AL10 9AB, Hatfield, United Kingdom
[82] University of Antwerp, Onderzoeksgroep Toegepaste Wiskunde, Middelheimlaan 1, 2020 Antwerp, Belgium
[83] INAF - Osservatorio Astronomico d'Abruzzo, Via Mentore Maggini, 64100 Teramo, Italy
[84] Instituto de Astronomia, Geofìsica e Ciências Atmosféricas, Universidade de São Paulo, Rua do Matão, 1226, Cidade Universitaria, 05508-900 São Paulo, SP, Brazil
[85] Mésocentre de calcul de Franche-Comté, Université de Franche-Comté, 16 route de Gray, 25030 Besançon Cedex, France
[86] SRON, Netherlands Institute for Space Research, Sorbonnelaan 2, 3584CA, Utrecht, The Netherlands
[87] Theoretical Astrophysics, Division of Astronomy and Space Physics, Department of Physics and Astronomy, Uppsala University, Box 516, 751 20 Uppsala, Sweden
[88] RHEA for European Space Agency (ESA), Camino bajo del Castillo, s/n, Urbanizacion Villafranca del Castillo, Villanueva de la Cañada, 28692 Madrid, Spain
[89] ATOS for CNES Centre Spatial de Toulouse, 18 avenue Edouard Belin, 31401 Toulouse Cedex 9, France
[90] School of Physics and Astronomy, Tel Aviv University, Tel Aviv 6997801, Israel
[91] Astrophysics Research Centre, School of Mathematics and Physics, Queen's University Belfast, Belfast BT7 1NN, UK
[92] Centre de Données Astronomique de Strasbourg, Strasbourg, France
[93] Université Côte d'Azur, Observatoire de la Côte d'Azur, CNRS, Laboratoire Géoazur, Bd de l'Observatoire, CS 34229, 06304 Nice Cedex 4, France
[94] Max-Planck-Institut für Astrophysik, Karl-Schwarzschild-Straße 1, 85748 Garching, Germany
[95] APAVE SUDEUROPE SAS for CNES Centre Spatial de Toulouse, 18 avenue Edouard Belin, 31401 Toulouse Cedex 9, France
[96] Área de Lenguajes y Sistemas Informáticos, Universidad Pablo de Olavide, Ctra. de Utrera, km 1. 41013, Sevilla, Spain
[97] Onboard Space Systems, Luleå University of Technology, Box 848, S-981 28 Kiruna, Sweden
[98] TRUMPF Photonic Components GmbH, Lise-Meitner-Straße 13,

[113] IRAP, Université de Toulouse, CNRS, UPS, CNES, 9 Av. colonel Roche, BP 44346, 31028 Toulouse Cedex 4, France
[114] Konkoly Observatory, Research Centre for Astronomy and Earth Sciences, MTA Centre of Excellence, Konkoly Thege Miklós út 15-17, 1121 Budapest, Hungary
[115] MTA CSFK Lendület Near-Field Cosmology Research Group, Konkoly Thege Miklós út 15–17, 1121 Budapest, Hungary
[116] ELTE Eötvös Loránd University, Institute of Physics, 1117, Pázmány Péter sétány 1A, Budapest, Hungary
[117] Ruđer Bošković Institute, Bijenička cesta 54, 10000 Zagreb, Croatia
[118] Institute of Theoretical Physics, Faculty of Mathematics and Physics, Charles University in Prague, Czech Republic
[119] INAF - Osservatorio Astronomico di Brera, via E. Bianchi 46, 23807 Merate (LC), Italy
[120] AKKA for CNES Centre Spatial de Toulouse, 18 avenue Edouard Belin, 31401 Toulouse Cedex 9, France
[121] Departmento de Física de la Tierra y Astrofísica, Universidad Complutense de Madrid, 28040 Madrid, Spain
[122] Vitrociset Belgium for European Space Agency (ESA), Camino bajo del Castillo, s/n, Urbanizacion Villafranca del Castillo, Villanueva de la Cañada, 28692 Madrid, Spain
[123] Department of Astrophysical Sciences, 4 Ivy Lane, Princeton University, Princeton NJ 08544, USA
[124] Departamento de Astrofísica, Centro de Astrobiología (CSIC-INTA), ESA-ESAC. Camino Bajo del Castillo s/n. 28692 Villanueva de la Cañada, Madrid, Spain
[125] naXys, University of Namur, Rempart de la Vierge, 5000 Namur, Belgium
[126] EPFL - Ecole Polytechnique fédérale de Lausanne, Institute of Mathematics, Station 8 EPFL SB MATH SDS, Lausanne, Switzerland
[127] H H Wills Physics Laboratory, University of Bristol, Tyndall Avenue, Bristol BS8 1TL, United Kingdom
[128] Sorbonne Université, CNRS, UMR7095, Institut d'Astrophysique de Paris, 98bis bd. Arago, 75014 Paris, France
[129] Porter School of the Environment and Earth Sciences, Tel Aviv University, Tel Aviv 6997801, Israel
[130] Laboratoire Univers et Particules de Montpellier, Université Montpellier, Place Eugène Bataillon, CC72, 34095 Montpellier Cedex 05, France
[131] Faculty of Mathematics and Physics, University of Ljubljana, Jadranska ulica 19, 1000 Ljubljana, Slovenia

Appendix A: *G*-band corrections for sources with 2-parameter or 6-parameter astrometric solutions

Figure A.1 shows how to formulate an ADQL query, to be executed in the *Gaia* EDR3 archive, that contains an on-the-fly calculation of the corrected *G*-band fluxes or magnitudes. These queries are somewhat complex and create a performance overhead. Hence downloading the requisite *Gaia* EDR3 fields and calculating the corrections a posteriori may be more efficient. Example Python code to do this is included in Fig. A.2. The Python code is also available as a Jupyter notebook at the following link: https://github.com/agabrown/gaiaedr3-6p-gband-correction.

Appendix B: Calculating the corrected flux excess factor

Figure B.1 shows how to formulate an ADQL query, to be executed in the *Gaia* EDR3 archive, that contains an on-the-fly calculation of the corrected flux excess factor. This query is somewhat complex and incurs a performance overhead. Hence downloading the requisite *Gaia* EDR3 fields and calculating the corrections a posteriori may be more efficient. Example Python code to do this is included in Fig. B.2. The Python code is also available as a Jupyter notebook at the following link: https://github.com/agabrown/gaiaedr3-flux-excess-correction.

Fig. A.1. Example queries that can be submitted to the *Gaia* archive in the Astronomical Data Query Language to retrieve corrected G-band photometry.

Query that includes a calculation of the G-band flux correction. The condition '`bp_rp > -20`' ensures that no correction is attempted in case the $(G_{\rm BP} - G_{\rm RP})$ colour is not available ('`bp_rp is not null`' does not work). The condition on `random_index` is included to retrieve example data for a random sample of sources.

```
select source_id, astrometric_params_solved, bp_rp, phot_g_mean_mag, phot_g_mean_flux,
if_then_else(
  bp_rp > -20,
  case_condition(
    phot_g_mean_flux * (1.00525 -0.02323*greatest(0.25, least(bp_rp, 3))
            +0.01740*power(greatest(0.25, least(bp_rp, 3)),2)
            -0.00253*power(greatest(0.25, least(bp_rp, 3)),3)),
    astrometric_params_solved = 31,
    phot_g_mean_flux,
    phot_g_mean_mag < 13,
    phot_g_mean_flux,
    phot_g_mean_mag < 16,
    phot_g_mean_flux * (1.00876 -0.02540*greatest(0.25, least(bp_rp, 3))
                   +0.01747*power(greatest(0.25, least(bp_rp, 3)),2)
                   -0.00277*power(greatest(0.25, least(bp_rp, 3)),3))
  ),
  phot_g_mean_flux
) as phot_g_mean_flux_corr
from gaiaedr3.gaia_source
where random_index between 1000000 and 1999999
```

Query that includes a calculation of the G-band magnitude correction. We note the type-cast '`to_real()`' of the return value of the conditional part of the query.

```
select source_id, astrometric_params_solved, bp_rp, phot_g_mean_mag, phot_g_mean_flux,
if_then_else(
  bp_rp > -20,
  to_real(case_condition(
    phot_g_mean_mag - 2.5*log10( (1.00525 -0.02323*greatest(0.25, least(bp_rp, 3))
                                  +0.01740*power(greatest(0.25, least(bp_rp, 3)),2)
                                  -0.00253*power(greatest(0.25, least(bp_rp, 3)),3)) ),
    astrometric_params_solved = 31,
    phot_g_mean_mag,
    phot_g_mean_mag < 13,
    phot_g_mean_mag,
    phot_g_mean_mag < 16,
    phot_g_mean_mag - 2.5*log10( (1.00876 -0.02540*greatest(0.25, least(bp_rp, 3))
                                  +0.01747*power(greatest(0.25, least(bp_rp, 3)),2)
                                  -0.00277*power(greatest(0.25, least(bp_rp, 3)),3)) )
  )),
  phot_g_mean_mag
) as phot_g_mean_mag_corr
from gaiaedr3.gaia_source
where random_index between 5000000 and 5999999
```

Fig. A.2. Python code for calculating the corrections to the *G*-band photometry for sources with 2-parameter or 6-parameter astrometric solutions.

```
import numpy as np

def correct_gband(bp_rp, astrometric_params_solved, phot_g_mean_mag, phot_g_mean_flux):
    """
    Correct the G-band fluxes and magnitudes for the input list of Gaia EDR3 data.

    Parameters
    ----------

    bp_rp: float, array_like
        The (BP-RP) colour listed in the Gaia EDR3 archive.
    astrometric_params_solved: int, array_like
        The astrometric solution type listed in the Gaia EDR3 archive.
    phot_g_mean_mag: float, array_like
        The G-band magnitude as listed in the Gaia EDR3 archive.
    phot_g_mean_flux: float, array_like
        The G-band flux as listed in the Gaia EDR3 archive.

    Returns
    -------

    The corrected G-band magnitudes and fluxes. The corrections are only applied to
    sources with a 2-parameter or 6-parameter astrometric solution fainter than G=13,
    for which a (BP-RP) colour is available.

    Example

    gmag_corr, gflux_corr = correct_gband(bp_rp, astrometric_params_solved,
                                          phot_g_mean_mag, phot_g_mean_flux)
    """
    if np.isscalar(bp_rp) or np.isscalar(astrometric_params_solved) or \
                    np.isscalar(phot_g_mean_mag) or np.isscalar(phot_g_mean_flux):
        bp_rp = np.float64(bp_rp)
        astrometric_params_solved = np.int64(astrometric_params_solved)
        phot_g_mean_mag = np.float64(phot_g_mean_mag)
        phot_g_mean_flux = np.float64(phot_g_mean_flux)

    if not (bp_rp.shape == astrometric_params_solved.shape \
                        == phot_g_mean_mag.shape == phot_g_mean_flux.shape):
        raise ValueError('Function parameters must be of the same shape!')

    do_not_correct = np.isnan(bp_rp) | (phot_g_mean_mag<13) | \
                                       (astrometric_params_solved == 31)
    bright_correct = np.logical_not(do_not_correct) & (phot_g_mean_mag>=13) & \
                                    (phot_g_mean_mag<=16)
    faint_correct = np.logical_not(do_not_correct) & (phot_g_mean_mag>16)
    bp_rp_c = np.clip(bp_rp, 0.25, 3.0)

    correction_factor = np.ones_like(phot_g_mean_mag)
    correction_factor[faint_correct] = 1.00525 - 0.02323*bp_rp_c[faint_correct] + \
        0.01740*np.power(bp_rp_c[faint_correct],2) - \
        0.00253*np.power(bp_rp_c[faint_correct],3)
    correction_factor[bright_correct] = 1.00876 - 0.02540*bp_rp_c[bright_correct] + \
        0.01747*np.power(bp_rp_c[bright_correct],2) - \
        0.00277*np.power(bp_rp_c[bright_correct],3)

    gmag_corrected = phot_g_mean_mag - 2.5*np.log10(correction_factor)
    gflux_corrected = phot_g_mean_flux * correction_factor

    return gmag_corrected, gflux_corrected
```

Fig. B.1. Example query that can be submitted to the *Gaia* archive in the Astronomical Data Query Language to retrieve the corrected flux excess factor presented in Riello et al. (2021).

Query that includes a calculation of the correction of the flux excess factor. The condition '`bp_rp > -20`' ensures that no correction is attempted in case the ($G_{BP} - G_{RP}$) colour is not available ('`bp_rp is not null`' does not work). We note the type-cast '`to_real()`' of the return value of the conditional part of the query. The condition on `random_index` is included to retrieve example data for a random sample of sources.

```
select source_id, bp_rp, phot_bp_rp_excess_factor,
if_then_else(
    bp_rp > -20,
    to_real(case_condition(
        phot_bp_rp_excess_factor - (1.162004 + 0.011464*bp_rp
                                    + 0.049255*power(bp_rp,2)
                                    - 0.005879*power(bp_rp,3)),
        bp_rp < 0.5,
        phot_bp_rp_excess_factor - (1.154360 + 0.033772*bp_rp
                                             + 0.032277*power(bp_rp,2)),
        bp_rp >= 4.0,
        phot_bp_rp_excess_factor - (1.057572 + 0.140537*bp_rp)
    )),
    phot_bp_rp_excess_factor
) as phot_bp_rp_excess_factor_corr
from gaiaedr3.gaia_source
where random_index between 1000000 and 1999999
```

Fig. B.2. Python code for calculating the corrected flux excess factor presented in Riello et al. (2021).

```
import numpy as np

def correct_flux_excess_factor(bp_rp, phot_bp_rp_excess_factor):
    """
    Calculate the corrected flux excess factor for the input Gaia EDR3 data.

    Parameters
    ----------

    bp_rp: float, array_like
        The (BP-RP) colour listed in the Gaia EDR3 archive.
    phot_bp_rp_flux_excess_factor: float, array_like
        The flux excess factor listed in the Gaia EDR3 archive.

    Returns
    -------

    The corrected value for the flux excess factor, which is zero for "normal" stars.

    Example
    -------

    phot_bp_rp_excess_factor_corr = correct_flux_excess_factor(bp_rp,
                                                phot_bp_rp_flux_excess_factor)
    """

    if np.isscalar(bp_rp) or np.isscalar(phot_bp_rp_excess_factor):
        bp_rp = np.float64(bp_rp)
        phot_bp_rp_excess_factor = np.float64(phot_bp_rp_excess_factor)

    if bp_rp.shape != phot_bp_rp_excess_factor.shape:
        raise ValueError('Function parameters must be of the same shape!')

    do_not_correct = np.isnan(bp_rp)
    bluerange = np.logical_not(do_not_correct) & (bp_rp < 0.5)
    greenrange = np.logical_not(do_not_correct) & (bp_rp >= 0.5) & (bp_rp < 4.0)
    redrange = np.logical_not(do_not_correct) & (bp_rp > 4.0)

    correction = np.zeros_like(bp_rp)
    correction[bluerange] = 1.154360 + 0.033772*bp_rp[bluerange] +
                                       0.032277*np.power(bp_rp[bluerange],2)
    correction[greenrange] = 1.162004 + 0.011464*bp_rp[greenrange] + \
                                        0.049255*np.power(bp_rp[greenrange],2) \
                                      - 0.005879*np.power(bp_rp[greenrange],3)
    correction[redrange] = 1.057572 + 0.140537*bp_rp[redrange]

    return phot_bp_rp_excess_factor - correction
```